

Geometry of the comptonization region of MAXI J1348–630 through type-C quasi-periodic oscillations with *NICER*

KEVIN ALABARTA,¹ MARIANO MÉNDEZ,² FEDERICO GARCÍA,³ DIEGO ALTAMIRANO,⁴ YUEXIN ZHANG,^{5,2} LIANG ZHANG,⁶ DAVID M. RUSSELL,¹
AND OLE KÖNIG^{7,8}

¹*Center for Astrophysics and Space Science (CASS), New York University Abu Dhabi,
PO Box 129188, Abu Dhabi, UAE*

²*Kapteyn Astronomical Institute, University of Groningen,
PO Box 800, NL-9700 AV Groningen, the Netherlands*

³*Instituto Argentino de Radioastronomía (CCT La Plata, CONICET; CICPBA; UNLP), C.C.5, (1894)
Villa Elisa, Buenos Aires, Argentina*

⁴*School of Physics and Astronomy, University of Southampton, Southampton, SO17 1BJ, UK*

⁵*Center for Astrophysics | Harvard & Smithsonian, 60 Garden Street, Cambridge, MA 02138, USA*

⁶*Key Laboratory of Particle Astrophysics, Institute of High Energy Physics, Chinese Academy of Sciences, Beijing 100049, China*

⁷*Center for Astrophysics | Harvard & Smithsonian, 60 Garden Street, Cambridge, MA 02138, USA*

⁸*Dr. Karl Remeis-Observatory and Erlangen Centre for Astroparticle Physics, Friedrich-Alexander-Universität Erlangen-Nürnberg,
Sternwartstr. 7, 96049 Bamberg, Germany*

(Received)

Submitted to ApJ

ABSTRACT

We use the rms and lag spectra of the type-C quasi-periodic oscillation (QPO) to study the properties of the Comptonisation region (aka corona) during the low/hard and hard-intermediate states of the main outburst and reflare of MAXI J1348–630. We simultaneously fit the time-averaged energy spectrum of the source and the fractional rms and phase-lag spectra of the QPO with the time-dependent Comptonization model $\nu\text{COMP}T\text{H}$. The data can be explained by two physically connected coronae interacting with the accretion disc via a feedback loop of X-ray photons. The best-fitting model consists of a corona of $\sim 10^3$ km located at the inner edge of the disc and a second corona of $\sim 10^4$ km horizontally extended and covering the inner parts of the accretion disc. The properties of both coronae during the reflare are similar to those during the *low/hard* state of the main outburst, reinforcing the idea that both the outburst and the reflare are driven by the same physical mechanisms. We combine our results for the type-C QPO with those from previous work focused on the study of type-A and type-B QPOs with the same model to study the evolution of the geometry of the corona through the whole outburst, including the reflare of MAXI J1348–630. Finally, we show that the sudden increase in the phase-lag frequency spectrum and the sharp drop in the coherence function previously observed in MAXI J1348–630 are due to the type-C QPO during the decay of the outburst and can be explained in terms of the geometry of the coronae.

Keywords: accretion, accretion discs – black hole physics – stars: black holes – X-rays: binaries – X-rays: individual (MAXI J1348-630)

1. INTRODUCTION

During an outburst, black hole low-mass X-ray binaries (BH LMXBs) show evolving spectral and timing properties (e.g., van der Klis 1989; Méndez & van der Klis 1997; van der Klis 2000; Homan & Belloni 2005; Remillard et al. 2006; Belloni 2010b; Belloni et al. 2011; Plant et al. 2014; Motta 2016). Taking into account these properties, two main spectral states are defined (see e.g., Tanaka 1989; van der Klis 1994): the

low/hard state (LHS) and the high/soft state (HSS). During the LHS, the X-ray emission of the system is dominated by a Comptonized component (hereafter corona) described by a hard power-law in the X-ray energy spectrum. In the HSS, the X-ray emission is dominated by the accretion disc and described by a multi-colour disc blackbody. Between the LHS and the HSS, it is possible to distinguish two intermediate states (Homan & Belloni 2005): the *hard-intermediate*

state (HIMS) and the *soft-intermediate state* (SIMS), showing properties in between the LHS and HSS.

In some BH LMXBs, at the end of the decay of an outburst, the X-ray luminosity increases again, reaching only up to 1–10% of the luminosity at the peak of the outburst. These events are known as “*reflares*” or “*rebrightenings*” (e.g., Callanan et al. 1995; Chen et al. 1997; Altamirano et al. 2011; Jonker et al. 2012; Patruno et al. 2016; Cúneo et al. 2020; Zhang et al. 2019, 2020a,b; Saikia et al. 2023). The similarities between the properties of BH LMXBs during outbursts and reflare suggest that both types of events are driven by the same physical processes (e.g., Patruno et al. 2016; Cúneo et al. 2020; Alabarta et al. 2022), although this is still not clear.

BH LMXBs show strong variability that evolves along the different spectral states. During the LHS, the power-density spectrum (PDS) of the system is characterised by strong broadband noise with a fractional rms amplitude of 30%–50% (e.g. Méndez & van der Klis 1997; Belloni et al. 2005; Remillard et al. 2006; Muñoz-Darias et al. 2011; Motta 2016). In contrast, in the HSS, the broadband fractional rms of BH LMXBs is generally less than 5% (Méndez & van der Klis 1997).

Low-frequency quasi-periodic oscillations (LF QPO) can also be detected in the PDS of a BH LMXB during outburst, with frequencies ranging from a few mHz to 30 Hz (e.g., Psaltis et al. 1999; Nowak 2000; Belloni et al. 2002; Casella et al. 2004; Belloni et al. 2005; Remillard & McClintock 2006; Belloni 2010a). Based on the combined properties of the QPO and the broadband noise components, these LF QPOs are classified into type-A, -B and -C (e.g., Wijnands et al. 1999; Casella et al. 2004, 2005). The type-C QPOs, which are the main point of this paper, consist of a strong and narrow peak with a centroid frequency ranging from 0.01 Hz to 30 Hz superposed to strong, 15–30% fractional rms amplitude, broadband noise component that can be decomposed into individual Lorentzians (e.g., Casella et al. 2004; Belloni et al. 2005). Type-C QPOs are detected both in the LHS and the HIMS.

The radiative origin of type-C QPOs can be determined by the study of their energy-dependent timing properties, such as the fractional rms amplitude (e.g., Tomsick & Kaaret 2001; Casella et al. 2004, 2005; Rodriguez et al. 2004b,a; Sobolewska & Życki 2006; Axelsson & Done 2016; Zhang et al. 2017, 2020c; Karpouzas et al. 2021; Ma et al. 2021) and the lags between different energy bands (e.g., Vaughan et al. 1994; Vaughan & Nowak 1997; Reig et al. 2000; Cui et al. 2000; Casella et al. 2004; Muñoz-Darias et al. 2010; Pahari et al. 2013; Zhang et al. 2017; Jithesh et al. 2019; Zhang et al. 2020c; Méndez et al. 2024).

The fractional rms amplitude of type-C QPOs increases with energy up to 10–20 keV and remains more or less con-

stant above that energy and up to ~ 200 keV (e.g., Casella et al. 2004; Zhang et al. 2017, 2020c; Ma et al. 2021). The high fractional rms values of type-C QPOs at energies above ~ 20 – 30 keV indicates that the corona dominates the QPO emission, supporting models that identify type-C QPOs as oscillations in the physical properties of the corona (e.g., Lee et al. 2001; Kumar & Misra 2014; Karpouzas et al. 2020; Bellavita et al. 2022).

Lags represent the delay between photons of two different energy bands. The lags are obtained from the Fourier cross-spectrum (CS) between the light curves in the subject and reference energy bands (e.g. van der Klis et al. 1996; Vaughan & Nowak 1997; Nowak et al. 1999). If the high-energy photons are delayed with respect to those from low-energy bands, the lags are defined as positive and are called *hard lags*. On the contrary, if the low-energy photons are delayed with respect to those from high-energy bands, the lags are defined as negative and are called *soft lags*. Both soft and hard lags have been observed for type-C QPOs of BH LMXBs (e.g., Reig et al. 2000; Cui et al. 2000; Casella et al. 2004; Muñoz-Darias et al. 2010; Pahari et al. 2013; Zhang et al. 2017; Jithesh et al. 2019; Zhang et al. 2020c).

The physical origin of these lags is still poorly understood, although several mechanisms have been proposed to explain them. Hard lags, for instance, could be produced by Comptonization of soft photons from the accretion disc in the corona (e.g., Payne 1980; Miyamoto et al. 1988; Nobili et al. 2000; Lee et al. 2001; Kumar & Misra 2014; Karpouzas et al. 2020), or propagating fluctuations of the mass accretion rate from the outer parts of the accretion disc to the inner parts and the corona (e.g., Arévalo & Uttley 2006; Ingram & van der Klis 2013). Soft lags, on the other hand, can be explained by the reverberation of photons from the corona impinging back in the accretion disc (e.g., Uttley et al. 2014; De Marco et al. 2015; Ingram & Motta 2020). Reverberation, however, cannot explain the lags of QPOs (De Marco et al. 2015). Alternatively, soft lags can be produced by Comptonization if one takes into account feedback between the corona and the accretion disc (Lee et al. 2001), in which a fraction of the up-scattered photons in the corona impinges back onto the accretion disc producing a time delay between the hard photons from the corona and those from the accretion disc (Karpouzas et al. 2020; Bellavita et al. 2022).

In addition to the lags, the CS also allows us to study the coherence function, which represents a measure of the linear correlation between the photons coming from the hard and the soft bands (Vaughan & Nowak 1997). Generally, in BH LMXBs, the coherence is consistent with ~ 1 in a broad range of frequencies, indicating that hard photons are strongly related to soft photons (e.g. Vaughan & Nowak 1997; Cui et al. 1997; Nowak et al. 1999; Ji et al. 2003). However, some drops in the coherence function at certain frequency ranges

have been observed (e.g., Cui et al. 1997; Nowak et al. 1999; Ji et al. 2003; Méndez et al. 2024; König et al. 2024). König et al. (2024) found a drop in the coherence function in *NICER* observations of Cyg X–1 at frequencies in between the two broad Lorentzian components describing the PDS of the system without finding a significant feature at the frequency of the drop in the PDS. These authors speculated that this drop was caused by a beat between the two broad Lorentzians. Alternatively, Méndez et al. (2024) observed a similar feature in the coherence function of MAXI J1820+070. Fitting the PDS and CS with the same multi-Lorentzian function, they found a Lorentzian only significant in the Imaginary part of the CS (called “Imaginary QPO” by Méndez et al. (2024)) at the same frequency as the drop in coherence. This suggested that both phenomena were produced by the same independent physical mechanism.

The X-ray timing properties of LMXBs also allow the study of the geometry of the corona and its evolution. As a result, recently, it has been shown that the size of the corona changes throughout the outburst (e.g., Kara et al. 2019; Wang et al. 2021b; García et al. 2022; Méndez et al. 2022; Zhang et al. 2023b). Several models have been proposed to explain the evolution of the geometry of the corona. An outflowing corona model was proposed to explain the correlation of the photon index characterising the corona with the broadband time lags and radio flux (e.g., Kylafis et al. 2008; Reig et al. 2018; Kylafis & Reig 2018; Kylafis et al. 2023). Alternatively, the corona has also been proposed to be the base of a jet emitted from the centre of the system (Markoff et al. 2005). The propagating mass accretion rate fluctuations assume a corona that lies over the inner parts of the accretion disc and is able to explain the broadband and QPO variability, as well as the energy spectra of LMXBs (Arévalo & Uttley 2006; Ingram & van der Klis 2013; Zdziarski et al. 2021; Kawamura et al. 2022). The family of RELTRANS models assume a lamppost geometry for the corona and measure its height with respect to the accretion disc by modelling the broadband lags due to reverberation (Ingram et al. 2019; Lucchini et al. 2023). The JED-SAD model (Ferreira 1997; Ferreira et al. 2006; Petrucci et al. 2008; Marcel et al. 2018a,b, 2019, 2020, 2022) assumes that the hard component of the X-ray emission can be described by a jet-emitting disc (JED) and the soft component by a standard accretion disc (SAD). This model explains the spectral and timing properties of LMXBs by changes in the geometry and the contribution of the JED and SAD components to the total X-ray emission.

Because they assume a monolithic time- and energy-dependent response function of the system (e.g., due to the accretion disc, Reynolds et al. 1999), all these models consider that the time lags are the result of a single process that leads to a single broadband variability component, the so-called broadband noise component, in the PDS and the CS of

these sources. Méndez et al. (2024), however, have recently shown that, as was already the case for the PDS (Nowak 2000; Belloni et al. 2002), the CS can also be decomposed in a number of Lorentzian functions (in this case, each of them multiplied by the cosine or sine of a frequency-dependent phase lag). This favours models of variability that consist of a number of response functions that act over well-defined time scales. This type of models includes Lense-Thirring precession (Ingram et al. 2009) and ν KOMPTH (Karpouzas et al. 2020; Bellavita et al. 2022).

This study focuses on the recently developed model ν KOMPTH (Karpouzas et al. 2020; Bellavita et al. 2022), which has been able to reproduce the rms and lag spectra of QPOs and measure the characteristic size of the corona around LMXBs (e.g., Karpouzas et al. 2020, 2021; García et al. 2021, 2022; Méndez et al. 2022; Zhang et al. 2022, 2023b; Rawat et al. 2023; Rout et al. 2023; Ma et al. 2023). The ν KOMPTH model considers that the coupled oscillation between the corona and the accretion disc, at the frequency of the QPO, produces the radiative properties of QPOs. This model allows us to link the behaviour of these properties with the coronal geometry of the system.

MAXI J1348–630 is an X-ray binary discovered with MAXI in January 2019 (Yatabe et al. 2019; Tominaga et al. 2020). The source was also detected with *Swift* (D’Elia et al. 2019a,b), *NICER* (Sanna et al. 2019), *INTEGRAL* (Cangemi et al. 2019), *ATCA* (Russell et al. 2019b), *iTelescope.Net* (Denisenko et al. 2019) and LCO (Russell et al. 2019a). Based on its spectral and timing properties studied with *NICER* data, Sanna et al. (2019) suggested that the compact object in this system is a BH. Later on, a more detailed study of the evolution of these properties during the whole outburst using *NICER* allowed to reinforce the identification of MAXI J1348–630 as a BH candidate (Zhang et al. 2020a).

In this paper, we present the evolution of the properties of the corona of MAXI J1348–630 using the version of the Comptonization model ν KOMPTH with two coronas, ν KDU-ALDK (García et al. 2021; Bellavita et al. 2022) on the type-C QPO detected in this system. In Section 2, we describe the observations and data analysis. In section 3, we show the best-fit parameters of the observations included in this study and present the parameters describing the corona in the different phases of the outburst. Finally, in section 4, we compare the coronal properties of MAXI J1348–630 in the main outburst with those in the reflare and with other LMXBs and from them, we infer the potential geometry of the two coronae. Finally, we also show the evolution of the geometry based on the studies of the three types of QPOs observed in MAXI J1348–630.

2. OBSERVATIONS & DATA ANALYSIS

Alabarta et al. (2022) published a complete timing analysis of the *NICER* observations in which a type-C QPO was observed. They analysed 37 observations with type-C QPOs and gave the ObsIDs and the properties of the QPO in their Table 1. In this section, we briefly describe the data processing and refer the reader to Alabarta et al. (2022) for the details.

2.1. Light curve and HID

To recreate the light curve and HID presented in Alabarta et al. (2022), we extracted a background-subtracted energy spectrum for each ObsID using the `NIBACKGEN3C50` background model (Remillard et al. 2022). We obtained the count rate of the source in the 0.5–12 keV, 2–3.5 keV and 6–12 keV energy bands for each ObsID, defined the intensity as the background-subtracted count rate in the 0.5–12 keV energy range and the hardness ratio as the ratio between the background-subtracted count rate of the 6–12 keV and 2–3.5 keV energy bands (one point per ObsID). Figure 1 shows the *NICER* light curve and hardness ratio vs time, and Figure 2 shows the HID of MAXI J1348–630. In both figures, we marked the observations with different symbols, showing type-A, -B, and -C QPOs.

2.2. Time-averaged energy spectra

We fitted the energy spectra of MAXI J1348–630 in the energy band 0.7 – 10 keV using XSPEC (V. 12.10.1; Arnaud 1996). We rebinned the spectra by a factor of 3 to correct for energy oversampling and then to have at least 25 counts per bin. In addition, we added a systematic error of 1% in the energy range 0.7 – 10 keV. We found strong instrumental residuals below 3 keV. These residuals are typical for X-ray missions with Si-based detectors (e.g. Ludlam et al. 2018; Miller et al. 2018). We, therefore, fitted those residuals with three `EDGE` and one `GABS` components, and ignored the 1.7 – 2.3 keV energy range. We fitted the energy spectra with an absorbed (`TBFE0` in XSPEC, Wilms et al. 2000) combination of a thermal Comptonisation model (Zdziarski et al. 1996; Życki et al. 1999) and a multi-colour disc blackbody, `TBFE0(NTHCOMP+DISKBB)`. In order to obtain the fluxes of the different components, we added two `CFLUX` components to the models. The solar abundances were set according to Wilms et al. (2000), and the hydrogen column density (N_H) of the `TBFE0` was left free. The cross-section was set according to Verner et al. (1996). The 1σ errors of the parameters were calculated from a Monte Carlo Markov Chain of length 240000 with a 2400-step burn-in phase.

First, we fitted all the energy spectra separately, linking the kT_{bb} parameter of `NTHCOMP` and kT_{in} of `DISKBB`. We found that the electron temperature, kT_e , in `NTHCOMP` was always above the maximum energy of the instrument. Therefore, we fixed kT_e at 50 keV. Besides, we noted that the values of the parameters of `TBFE0` in all the fitted energy spectra were

consistent within errors. For this reason, we decided to fix N_H to $0.86 \times 10^{22} \text{ cm}^{-2}$ as in Carotenuto et al. (2021), link the parameters O and Fe in all the spectra and to repeat the fitting.

The fit with this model shows significant residuals at 6–7 keV. These residuals are thought to be due to the reflection component (e.g., García et al. 2014; Fabian et al. 1989). Therefore, we added to the model the relativistic reflection component, `RELXILLCP` (version 1.4.3; Dauser et al. 2014). It is necessary to point out that the seed photons in `RELXILLCP` correspond to the Comptonized `NTHCOMP` spectrum of a disc-blackbody with a fixed temperature of $kT_{in} = 0.01$ keV. This spectrum is very different from that of LMXBs, in which the typical disc-blackbody temperatures range between 0.5 keV and 2 keV. This introduces a bias in the spectral modelling, producing a soft excess at ~ 2 keV. In order to correct for this soft excess, we normalised this component by the ratio between an `NTHCOMP` model evaluated at $kT_b = kT_{in}$ and the `NTHCOMP` at 0.05 keV, using the so-called `NTHRATIO` model¹. We note that `NTHRATIO` takes no extra degrees of freedom because all of its parameters are linked to the corresponding parameters of `NTHCOMP`. We linked kT_e and Γ in `RELXILLCP` with the corresponding parameters kT_e and Γ in `NTHCOMP`. We then fixed the BH spin, a_* , at 0.998. In all the observations, we also linked the inclination, i , and iron abundance, A_{Fe} . In order to get only the reflected emission of `RELXILLCP`, we fixed the reflection fraction to -1 . We set the disc inner radius, R_{in} , at the ISCO, linked the emissivity indices of the `relxillcp`, α_1 , and α_2 , to be the same, and we let the ionisation parameter, ξ , and the normalisation of `RELXILLCP` free.

2.3. PDS, rms and lag spectra, and coherence function

The representative PDS of the observations of MAXI J1348–630 were presented in Figure 3 of Alabarta et al. (2022) and the properties of the type-C QPO were shown in Table 1 of Alabarta et al. (2022). All the PDS were fitted with a multi-Lorentzian function, using the characteristic frequency of the Lorentzians defined in Belloni et al. (2002), $\nu_{max} = \sqrt{\nu_0 + (FWHM/2)^2} = \nu_0 \sqrt{1 + 1/4Q^2}$, where $FWHM$ is the full width at half maximum, ν_0 the centroid frequency of the Lorentzian and the quality factor Q is defined as $Q = \nu_0/FWHM$. In Alabarta et al. (2022), we followed these criteria to identify the QPO: if there was only one narrow component, we identified it as the QPO. If there were two or more narrow Lorentzians, we assumed that the fundamental QPO was the strongest and narrowest Lorentzian and if the other narrow Lorentzians were at frequencies $\sim 1/2$ or ~ 2 times the frequency of the QPO, these Lorentzians were identified as the subharmonic or the harmonic, respectively.

¹ <https://github.com/garciafederico/nthratio>

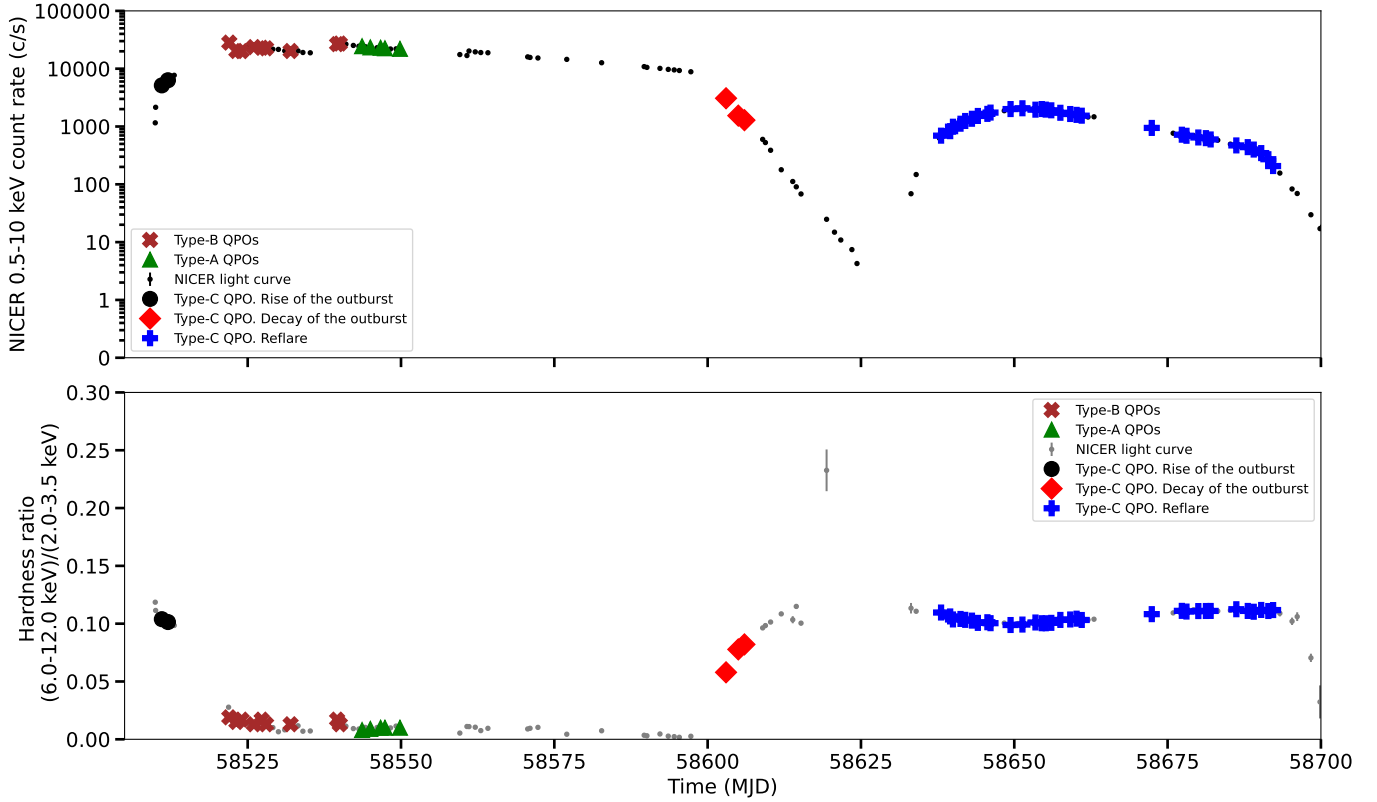


Figure 1. *NICER* light curve (top panel) and hardness ratio vs. time (bottom panel) of MAXI J1348–630. Black, red and blue symbols represent the observations corresponding, respectively, to the rise, decay and first reflare of the outburst in which type-C QPOs were observed. Brown and green symbols represent, respectively, the observations in which type-B (Belloni et al. 2020) and type-A QPOs (Zhang et al. 2023a) were detected. Grey symbols represent the rest of the *NICER* light curve (top panel) and the rest of the temporal evolution of the hardness ratio (bottom panel).

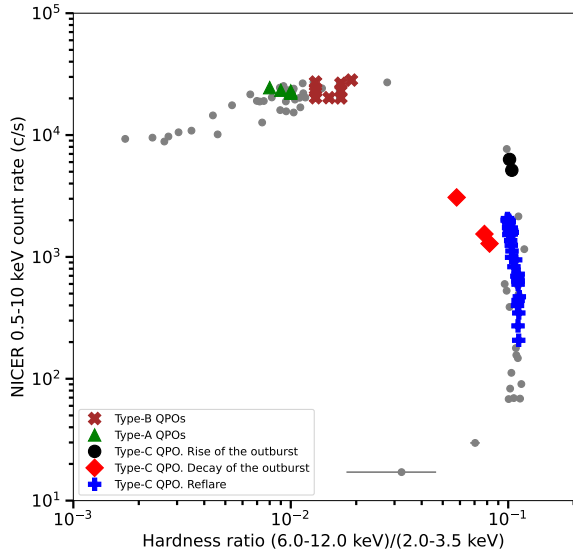


Figure 2. Hardness-intensity diagram (HID) of MAXI J1348–630. Colours and symbols are the same as in Fig. 1.

To obtain the rms spectrum, Alabarta et al. (2022) carried out the procedure described above in the following energy

bands: 0.5 – 1.0 keV, 1.0 – 1.5 keV, 1.5 – 2.0 keV, 2.0 – 3.0 keV, 3.0 – 4.0 keV, 4.0 – 6.0 keV, 6.0 – 8.0 keV and 8.0 – 12.0 keV.

In order to compute the phase-lag spectrum of the Lorentzian associated with the type-C QPO, Alabarta et al. (2022) produced the CS using the selected subject bands listed above and 0.5–12 keV as the reference band. They fit simultaneously the Real and Imaginary parts of each cross-spectrum in XSPEC using the multi-Lorentzian model used to fit the PDS, with the centroid frequencies and FWHM of each Lorentzian in the model fixed, letting their normalisations vary. Next, the phase-lag of the fundamental QPO was calculated by taking the arctan of the ratio of the normalization of the Lorentzians associated with the Imaginary and Real parts of the QPO, respectively, $\phi = \text{atan}(\text{Im}(\text{QPO})/\text{Re}(\text{QPO}))$.

This method has also been used in Peirano et al. (2023); Zhang et al. (2023b); Ma et al. (2023) and fully developed in Méndez et al. (2024). In particular, the analysis in Alabarta et al. (2022) corresponds to the case of the constant phase-lag model in Méndez et al. (2024). To compute the broadband phase lags and coherence function vs. frequency

in Section 3.3, we selected 0.5–2.0 keV and 2.0–10.0 keV as the reference and subject energy bands, respectively.

2.4. Joint fitting of the time-averaged, rms and phase-lag spectra

We fit the time-average spectra of the source, and the fractional rms and the phase-lag spectra of the type-C QPO simultaneously. For the energy spectra of the source, we used the model described in Section 2.2. For the fractional rms and phase-lag spectra of the QPO, we used the time-dependent Comptonization model `vkompth` presented in [Karpouzas et al. \(2020\)](#) and [Bellavita et al. \(2022\)](#). This model assumes that the QPO is a small oscillation around the solution of the stationary Kompaneets equation ([Kompaneets 1957](#)), which describes the energy spectrum of the system. This model allows us to link the behaviour of the energy-dependent phase-lags and fractional rms amplitude with the physical properties of the system.

Initially, we considered the version of `vkompthdk` for one corona. This model considers that the seed photon source is a geometrically thin, optically thick accretion disc ([Shakura & Sunyaev 1973](#)) with a temperature kT_s , surrounded by a corona of hot electrons with temperature kT_e , where the seed photons are inverse-Compton scattered. This corona is assumed to be spherically symmetric with a size L and constant optical depth τ . The model also includes feedback from the up-scattered photons in the corona to the seed photon source. This feedback is described by the parameter called “feedback-fraction”, η , whose values range between 0 and 1, and is given by

$$\eta = \frac{F_{\text{disc}} - F_{\text{disc},0}}{F_{\text{disc}}}$$

where F_{disc} is the total flux of the disc and $F_{\text{disc},0}$ represents the flux of the disc before the corona illuminates it. In summary, η represents the fraction of the disc flux produced by the feedback process. The parameter η , in turn, is related to η_{int} (intrinsic feedback fraction; see [Karpouzas et al. 2020](#)), where η_{int} is defined as the fraction of the coronal flux that illuminates the disc. In addition to these parameters, `vkompthdk` also considers an unspecified external heating source of the corona, $\delta\dot{H}_{\text{ext}}$, and an additive parameter, *reflag*, that gives the phase lag in the 2–3 keV band. We also added a *dilution* correction factor (defined as $\text{NTHCOMP}/(\text{NTHCOMP}+\text{DISKBB}+\text{RELXILLCP})$) that takes into account the effect of the non-variable emission on the fractional rms amplitude. By doing this, we are assuming that all the variability of the system originates from the Comptonized component.

During the fit, kT_s , kT_e and Γ of `vkompthdk` are linked to the corresponding parameters of `DISKBB` (kT_s), and `NTHCOMP` (kT_e and Γ). We found that fitting one corona cannot reproduce the rms and phase-lag spectra of MAXI J1348–630.

Table 1. Table of the *NICER* observations analysed in this work. From observation 6, the ObsIDs within the interval in the second column were used to produce the energy, rms and lag spectra.

Obs number	ObsID	QPO freq. (Hz)	Phase of the outburst
1	1200530103	0.45±0.04	Rise
2	1200530104	0.53±0.01	Rise
3	2200530127	2.93±0.04	Decay
4	2200530128	1.67±0.06	Decay
5	2200530129	1.56±0.06	Decay
6	2200530145–2200530147	0.60±0.04	Reflare
7	2200530148–2200530149	0.88±0.04	Reflare
8	2200530151–2200530162	0.94±0.01	Reflare
9	2200530165–2200530166	0.73±0.03	Reflare
10	2200530171–2200530186	0.40±0.01	Reflare

Because of this, we also fit the spectra with two Comptonization regions (e.g., [García et al. 2021](#); [Bellavita et al. 2022](#)) using the model `vkdualdk` ([Bellavita et al. 2022](#)). The two coronae (hereafter called corona 1 and corona 2) are assumed to be small and large, respectively, and described by two sets of parameters similar to those of the case of one corona: $kT_{s,1}$ and $kT_{s,2}$, $kT_{e,1}$ and $kT_{e,2}$, L_1 and L_2 , η_1 and η_2 , and $\delta\dot{H}_{\text{ext},1}$ and $\delta\dot{H}_{\text{ext},2}$. For simplicity, we assume that the photon index and kT_e of both coronae are equal. On the other hand, $kT_{s,1}$ is linked to kT_{in} on `DISKBB` and $kT_{s,2}$ is set as a free parameter. The 1σ errors of the parameters were calculated from a Markov Chain Monte Carlo of length 240000 with a 2400-step burn-in phase.

3. RESULTS

3.1. Fit to the energy spectra

We first fitted simultaneously all the observations of MAXI J1348–630 showing a type-C QPO (see Table 1 in [Alabarta et al. \(2022\)](#)). In order to increase the signal-to-noise ratio of the rms and phase-lags spectra of the QPO during the reflare, we combined all the observations with similar timing and spectral properties, resulting in a total of five energy spectra during the reflare of MAXI J1348–630 (see Table 1). We obtained a relatively good fit, with a χ^2/dof of 1.13, for 1884 degrees of freedom (for a total of 10 spectra).

The best-fitting parameters and their evolution are given in table 2. As stated in Section 2, we fixed the N_H at $0.86 \times 10^{22} \text{ cm}^{-2}$ and got for the oxygen and iron abundances of the interstellar medium along the line of sight $O=0.8 \pm 0.2$ and $F_e=0.34 \pm 0.02$. We obtained an inclination of $i=49.445^\circ \pm 0.001^\circ$, which is slightly higher than the estimations of previous studies (e.g., [Carotenuto et al. 2022](#); [Alabarta et al. 2022](#)).

The observations showing a type-C QPO during the rise of the outburst of MAXI J1348–630 show $\Gamma \sim 1.6$ and an inner-disc temperature of ~ 0.5 keV. During the HIMS, the photon index and the disc temperature decrease, respectively, from ~ 2.5 to ~ 2.0 and from ~ 0.3 keV to ~ 0.2 keV. Finally,

during the reflare, the photon index remains constant at ~ 1.7 . In contrast, kT_{in} increases from 0.24 keV at the beginning of the reflare to 0.36 keV at its peak and, after that, decreases until 0.25 keV at the last energy spectrum of the reflare.

3.2. Evolution of the parameters describing the corona

We then simultaneously fitted the energy spectrum of the source and the rms and phase-lag spectra of the QPO for each observation (or combination of observations, as explained in Section 3.1).

Figure 3 shows three representative joint fits of each phase of the outburst: rise and decay of the main outburst in, respectively, black and red, and the reflare in blue. The best-fitting parameters are given in Table 2, and the time evolution of the parameters is shown in Figure 4.

During the rise and the decay of the main outburst, kT_s decreases from 0.38 ± 0.03 keV to 0.087 ± 0.003 keV. During the reflare, kT_s initially increases from 0.092 ± 0.008 keV at the beginning to 0.17 ± 0.03 keV just after the peak. The last observation shows a slight decrease of kT_s to 0.13 ± 0.02 keV; however, the last two values are consistent within errors.

The size of the small corona, L_1 , initially decreases from ~ 6300 km ($\sim 425R_g$, all sizes in R_g units are for a BH of $10M_\odot$) to ~ 760 km ($\sim 51R_g$) during the observations corresponding to the rise of the main outburst. During the decay, L_1 increases from ~ 45 km ($\sim 3R_g$) to ~ 1000 km ($\sim 68R_g$). Finally, during the reflare, L_1 decreases from ~ 3550 km ($\sim 240R_g$) in Obs 6 to ~ 740 km ($\sim 50R_g$) in Obs 9. In the last observation, the upper limit to the size of the small corona is < 3000 km ($\sim 200R_g$). The feedback fraction of this corona, η_1 , ranges from 0.50 ± 0.09 to 0.96 ± 0.20 . However, their relatively large errors make all the values consistent with each other.

On the other hand, the size of the large corona, L_2 , is ~ 39000 km ($\sim 2600R_g$) in Obs 1 and less than ~ 55000 km ($\sim 3700R_g$) in Obs 2, both during the rise of the main outburst. During the decay, L_2 increases from ~ 660 km ($\sim 45R_g$) in Obs 3 to ~ 44000 km ($\sim 3000R_g$) in Obs 4, while it decreases to ~ 7300 km ($\sim 500R_g$) in Obs 5. Finally, during the reflare, L_2 increases from ~ 14500 km ($\sim 980R_g$) to a value ranging between ~ 52800 km ($\sim 3600R_g$) and ~ 63000 km ($\sim 4200R_g$). Obs 9 shows an L_2 of ~ 22000 km ($\sim 1500R_g$), which is lower than that of the observations before and after. The feedback fraction of this corona, η_2 , shows different values depending on the phase of the outburst. During the rise of the main outburst, we got only upper limits for η_2 , < 1.00 and < 0.73 , for Obs 1 and Obs 2, respectively. During the reflare, η_2 increases from ~ 0.75 in Obs 6 to ~ 1.00 in Obs 7, 8 and 9, while in Obs 10, η_2 is 0.55. During the decay of the main outburst, the values for η_2 are lower than those during the rise of the main outburst and the reflare, ranging between < 0.03 and ~ 0.3 . The values corresponding to the intrinsic feedback

fraction are, for the small corona, $\eta_{int,1} \sim 0.03$ in the rise and the reflare of the outburst and $\eta_{int,1} \sim 0.15$ in the decay of the outburst. The parameter $\eta_{int,2}$, on the other hand, is ~ 0.02 during the rise and the reflare and ~ 0.07 during the decay of the outburst.

Figure 5 shows the evolution of the sizes of the two coronae with the flux ratio (left panel) and the QPO frequency (right panel), respectively. We found that both L_1 and L_2 decrease as the QPO frequency and the flux ratio increase. However, L_2 shows a higher scatter than L_1 in both cases.

3.3. Broadband phase-lags and coherence vs. frequency

In Alabarta et al. (2022), we studied the properties of the type-C QPO observed in MAXI J1348–630, and in the previous sections, we fitted the model `VKDUALDK` to the fractional rms and phase lags spectra of the type-C QPO. Inspired by the recent works of Méndez et al. (2024) and König et al. (2024), we decided to study the characteristics of the phase lags and the coherence function in two broad energy bands, 0.5–2.0 keV and 2.0–10.0 keV, vs. frequency of those observations showing a type-C QPO. Figures 6 and 7 show the PDS (top panels), the phase lags (middle panels) and coherence (bottom panels) vs. frequency. During the rise of the main outburst and the reflare, both in the LHS, the broadband phase lags are more or less constant at ~ 0.1 rad, with small excursions (less than 0.1 rad) at frequencies at which there is a feature in the PDS (Figure 6, middle panels). At the same time, the coherence function is consistent with being ~ 1 up to ~ 10 Hz, where the errors increase significantly (Figure 6, bottom panels). In particular, the coherence is ~ 1 at the frequency corresponding to the type-C QPO (orange line in Figure 6). On the contrary, during the decay of the main outburst, there is a sudden increase in the phase lags (Figure 7, middle panels) at the frequency of the QPO (also called “the cliff”; see Bellavita et al. 2024, in preparation) while the coherence function (Figure 7, bottom panels) drops at that frequency (orange line in Figure 7).² These sudden changes in both the lag and coherence are only observed in the three observations of the decay that show a type-C QPO in the PDS.

4. DISCUSSION

We found that the rms and lag spectra of the type-C QPO detected in MAXI J1348–630 with *NICER* during its 2019 outburst and its reflare can be explained in terms of two independent but physically coupled Comptonization regions. We jointly fit the time-average spectrum of the source and the rms and phase-lag spectra of the QPO with the time-dependent Comptonization model `VKDUALDK` (Karpouzas et al. 2020; Bellavita et al. 2022) and deduced the size and the feedback

² König et al. (2024) already showed this feature in ObsID 2200530129.

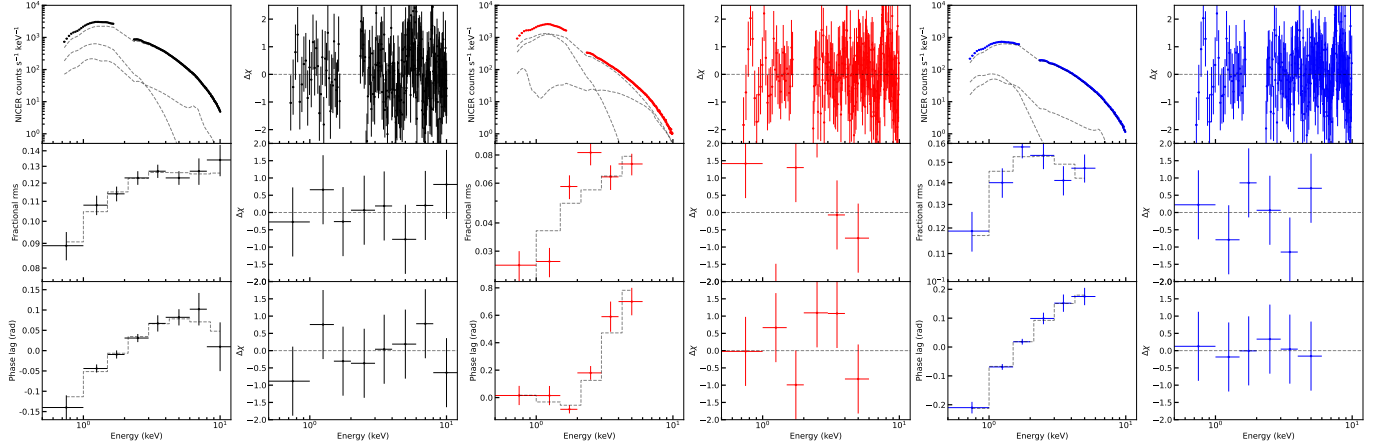


Figure 3. Three representative examples of the joint fitting of the time-averaged spectrum of the source (top), the fractional rms (middle) and lag spectra (bottom) of the type-C QPO during the rise (first column), decay (third column) and the reflare (fifth column) of MAXI J1348–630. The second, fourth, and sixth columns show the residuals of the fits in the panel on the left side of each residual. Black, red, and blue symbols represent the data corresponding to the rise, decay and first reflare of the outburst, respectively.

Table 2. Summary of the best-fitting parameters of the spectrum of the source and the rms and lag spectra of the type-C QPO in MAXI J1348–630 in the 0.5–10 keV energy band. Errors represent the 1σ level confidence interval of the parameter, while the upper limits represent the 95% confidence upper bound of the corresponding parameter.

	Obs 1	Obs 2	Obs 3	Obs 4	Obs 5	Obs 6	Obs 7	Obs 8	Obs 9	Obs 10
N_{H}	0.86*	0.86*	0.86*	0.86*	0.86*	0.86*	0.86*	0.86*	0.86*	0.86*
O	0.77*	0.77*	0.77*	0.77*	0.77*	0.77*	0.77*	0.77*	0.77*	0.77*
F_{c}	0.34*	0.34*	0.34*	0.34*	0.34*	0.34*	0.34*	0.34*	0.34*	0.34*
$\text{Flux}_{\text{disc}}$	$(2.19 \pm 0.05) \cdot 10^{-9}$	$(4.17 \pm 0.05) \cdot 10^{-9}$	$(4.09 \pm 0.07) \cdot 10^{-9}$	$(1.02 \pm 0.02) \cdot 10^{-9}$	$(0.93 \pm 0.02) \cdot 10^{-9}$	$(0.0511 \pm 0.0006) \cdot 10^{-9}$	$(0.21 \pm 0.01) \cdot 10^{-9}$	$(0.897 \pm 0.004) \cdot 10^{-9}$	$(0.676 \pm 0.008) \cdot 10^{-9}$	-
kT_{in}	0.465 ± 0.004	0.514 ± 0.003	0.328 ± 0.003	0.218 ± 0.002	0.201 ± 0.002	0.17 ± 0.01	0.239 ± 0.003	0.362 ± 0.001	0.349 ± 0.002	0.254 ± 0.006
$\text{Flux}_{\text{Comp}}$	$(26.2 \pm 0.2) \cdot 10^{-9}$	$(27.6 \pm 0.4) \cdot 10^{-9}$	$(7.60 \pm 0.04) \cdot 10^{-9}$	$(5.29 \pm 0.01) \cdot 10^{-9}$	$(4.71 \pm 0.01) \cdot 10^{-9}$	$(4.79 \pm 0.01) \cdot 10^{-9}$	$(6.44 \pm 0.06) \cdot 10^{-9}$	$(8.68 \pm 0.02) \cdot 10^{-9}$	$(7.99 \pm 0.02) \cdot 10^{-9}$	$(8.71 \pm 0.06) \cdot 10^{-9}$
Γ	1.643 ± 0.004	1.571 ± 0.004	2.52 ± 0.03	2.347 ± 0.01	2.009 ± 0.007	1.675 ± 0.001	1.69 ± 0.003	1.691 ± 0.001	1.659 ± 0.002	1.691 ± 0.001
kT_{c}	50*	50*	50*	50*	50*	50*	50*	50*	50*	50*
Index_1	1.49 ± 0.13	$10^{+0.009}_{-0.43}$	4.05 ± 0.18	4.15 ± 0.08	2.91 ± 0.08	7.78 ± 0.02	7.42 ± 0.22	1.35 ± 0.06	$-10^{+7.89}_{-0.17}$	1.35 ± 0.01
a	0.998	0.998	0.998	0.998	0.998	0.998	0.998	0.998	0.998	0.998
i	49.417	49.417	49.417	49.417	49.417	49.417	49.417	49.417	49.417	49.417
$\log x_1$	2.48 ± 0.02	42.1 ± 0.1	0.330 ± 0.001	3.29 ± 0.04	22.9 ± 0.2	68.8 ± 0.6	91.7 ± 0.6	41.1 ± 0.1	2.47 ± 0.08	2.0 ± 0.2
A_{Fe}	3.28 ± 0.26	$9.25^{+0.6}_{-1.49}$	0.50 ± 0.02	0.50 ± 0.01	0.50 ± 0.02	3.670 ± 0.008	$10^{+0.03}_{-1.44}$	0.54 ± 0.01	0.50 ± 0.03	0.541 ± 0.002
Norm_{ref}	0.020 ± 0.003	0.042 ± 0.004	0.20 ± 0.02	0.099 ± 0.005	0.019 ± 0.001	0.005090 ± 0.000006	0.0052 ± 0.0002	0.0111 ± 0.0009	0.0098 ± 0.0002	0.011 ± 0.001
kT_{e2}	0.38 ± 0.03	0.26 ± 0.06	0.18 ± 0.02	0.17 ± 0.01	0.087 ± 0.003	0.092 ± 0.008	0.11 ± 0.01	0.13 ± 0.02	0.17 ± 0.03	0.228 ± 0.003
L_1	6313^{+1404}_{-1149}	764^{+487}_{-252}	45^{+25}_{-15}	101^{+279}_{-272}	448^{+131}_{-77}	3548^{+923}_{-567}	2014^{+873}_{-627}	1798^{+784}_{-599}	742^{+302}_{-196}	5111^{+2388}_{-1242}
L_2	39200^{+357}_{-9303}	28754^{+239}_{-8406}	662^{+275}_{-220}	44400^{+3199}_{-8367}	7275^{+1257}_{-836}	14500^{+877}_{-578}	62900^{+16056}_{-10373}	54800^{+8277}_{-3085}	21900^{+1863}_{-7230}	17433^{+9288}_{-4047}
η_1	$0.62^{+0.2}_{-0.16}$	0.81 ± 0.16	0.67 ± 0.04	0.79 ± 0.08	0.50 ± 0.09	0.89 ± 0.02	0.74 ± 0.13	$0.92^{+0.03}_{-0.11}$	0.96 ± 0.20	0.89 ± 0.03
η_2	< 1.00	< 0.73	0.3 ± 0.04	< 0.03	0.27 ± 0.08	0.73 ± 0.02	0.99 ± 0.33	0.99 ± 0.13	0.55 ± 0.15	0.99 ± 0.01
$\delta\dot{H}_{\text{ext1}}$	$1.59^{+0.003}_{-0.19}$	0.53 ± 0.21	1.07 ± 0.27	1.06 ± 0.29	0.72 ± 0.14	0.78 ± 0.05	0.73 ± 0.15	0.17 ± 0.02	0.911 ± 0.27	1.49 ± 0.01
$\delta\dot{H}_{\text{ext2}}$	$0.38^{+0.1}_{-0.05}$	0.12 ± 0.05	0.84 ± 0.25	$0.82^{+0.09}_{-0.31}$	$0.98^{+0.005}_{-0.26}$	1.49 ± 0.07	$2.46^{+0.95}_{-0.74}$	$0.29^{+0.12}_{-0.27}$	$0.403^{+0.27}_{-0.04}$	0.72 ± 0.11
χ^2/ν	249.21/196	227.39/197	233.85/192	221.84/196	242.76/190	205.58/192	220.44/190	888.78/852	230.09/197	211.42/196

fraction of the coronae in the three phases of the outburst (rise, decay and reflare). This is the first time that the geometry of the coronae has been studied during a reflare of an LMXB. During the LHS of the main outburst and during the reflare (where the source always remains in the LHS), the size of the small corona is of the order of $\sim 10^2$ – 10^3 km with a feedback-fraction of >0.6 . In comparison, the larger corona is of the order of $\sim 10^4$ km with a high feedback fraction (>0.6). During the HIMS in the decaying part of the outburst, on the other hand, the large corona shows a lower

feedback fraction ($\eta_2 < 0.4$). In addition, we found that the sudden increase of the phase lags with Fourier frequency, the so-called cliff, in the phase lag frequency spectrum, and the drop in the coherence function previously reported by König et al. (2024) occur at the frequency of the type-C QPO in the three observations during the decay of the outburst.

4.1. Geometry of the coronae

During the rise of the main outburst (black circles in Fig. 4) and during the reflare (blue filled plusses in Fig. 4), the

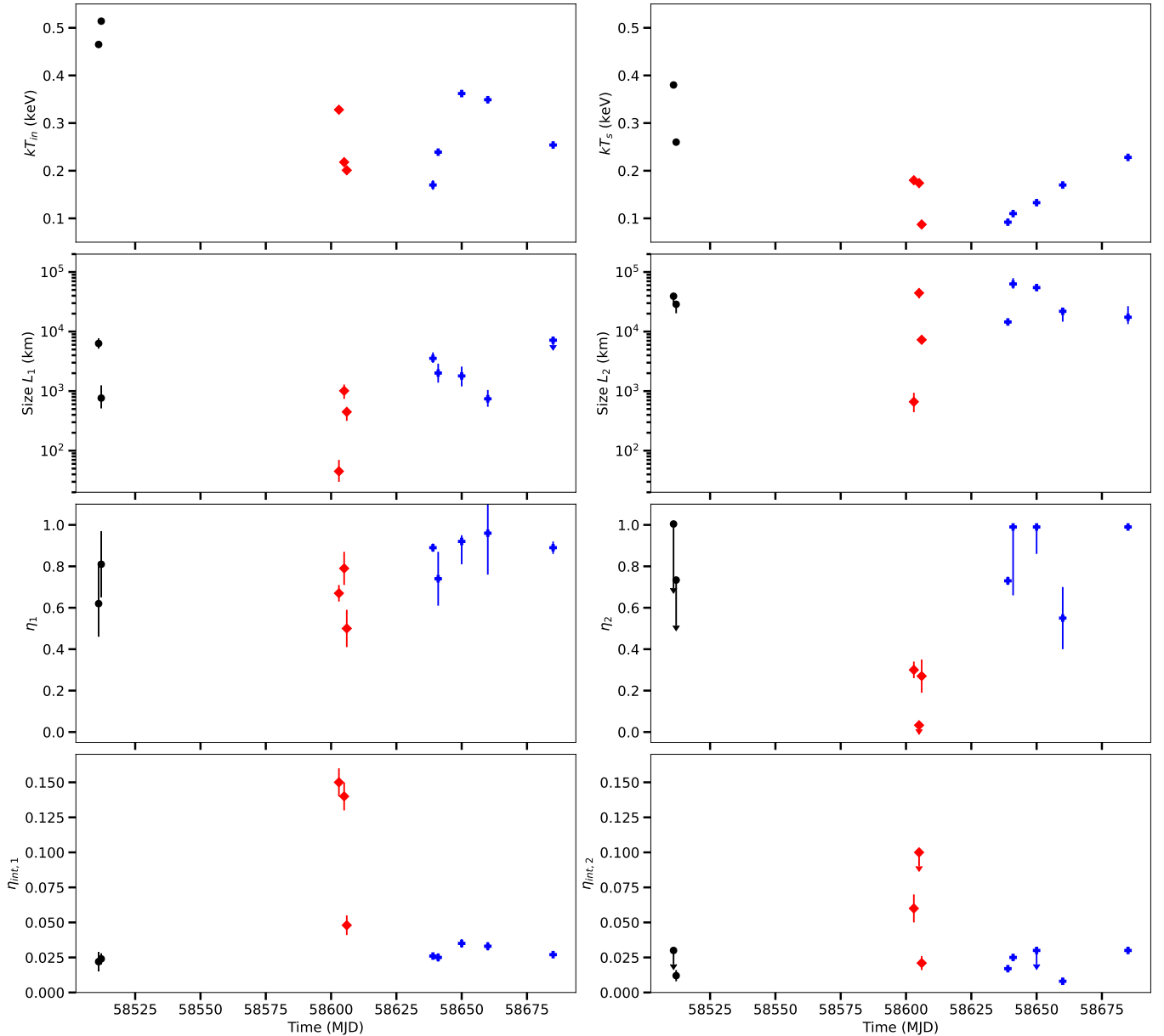


Figure 4. Evolution of the properties of the corona of MAXI J1348–630. The different colours represent the different phases of the outburst as defined in the previous figures.

size of the small corona, L_1 , ranges between $\sim 51R_g$, (for a BH of $10M_\odot$) and $\sim 425R_g$. The large corona, on the other hand, shows sizes ranging from $\sim 980R_g$ to $\sim 4250R_g$. During the decay of the main outburst (red diamonds in Fig. 4), MAXI J1348–630 was found to be in the HIMS (e.g., Zhang et al. 2020a; Alabarta et al. 2022). In the three observations in this state where a type-C QPO was found, L_1 increases from $\sim 3R_g$ to $\sim 70R_g$, while L_2 shows values between $20R_g$ and $1500R_g$.

In addition, the feedback fraction of both coronae provides a hint of their geometries. A high value of the feedback fraction suggests that the corona must be covering the accretion disc,

such that a large fraction of the disc flux originates from the Comptonised photons that return from the corona to the disc. A possible geometry for this scenario is a corona extending horizontally parallel to the accretion disc. On the contrary, a low value of the feedback fraction implies that the disc flux produced by photons that impinge back from the corona is not very large. Two potential geometries can explain low feedback values. The first one is a small corona located around the compact object with a size L smaller than the inner radius of the disc. The second one is a vertically extended corona, no matter its size, possibly moving away from the disc. During the rise of the main outburst and the reflare, both η_1 and η_2

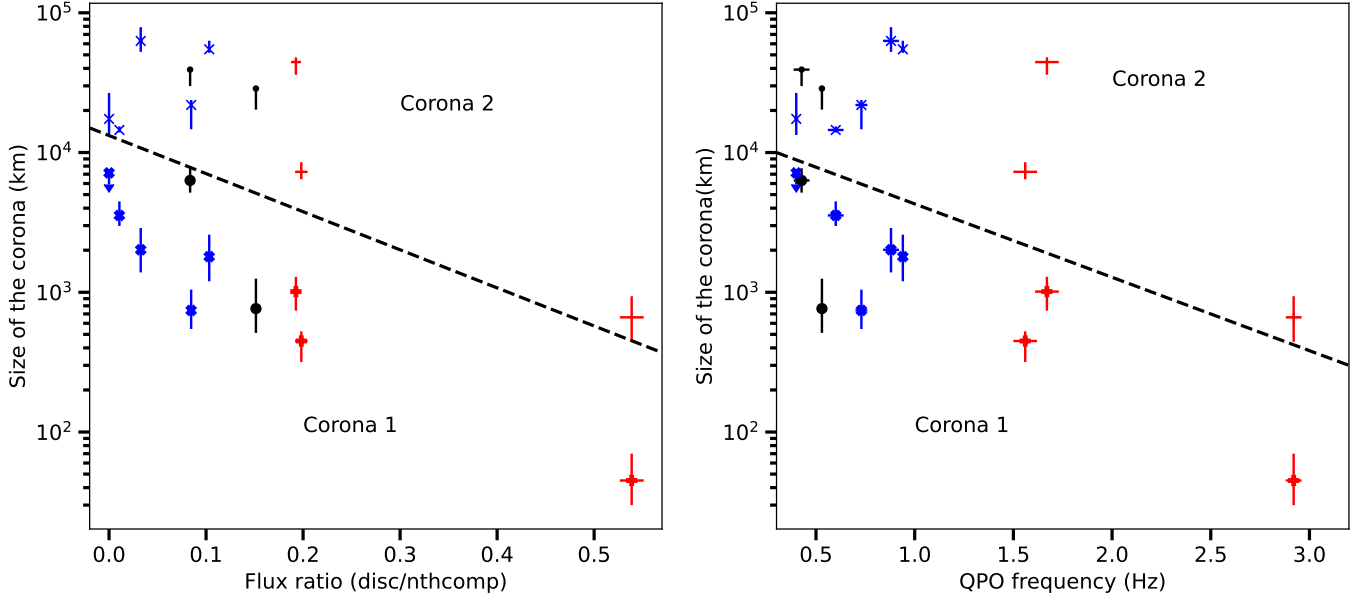


Figure 5. Evolution of the sizes of the small, L_1 and large corona, L_2 , with the flux ratio (left panel) and the QPO frequency (right panel). The different colours represent the different phases of the outburst, as defined in the previous figures. The dashed line separates the data of both coronae.

range between ~ 0.5 and ~ 1.0 . Considering that the sizes of the small and the large corona are, respectively, $L_1 \sim 10^2 - 10^3 R_g$ and $L_2 \sim 10^3 - 10^4 R_g$, we interpret that the two coronae are horizontally extended in the direction of the accretion disc, one being larger than the other one. The fact that the geometry is similar during both the rise of the outburst and the reflare reinforces the idea that both events are driven by the same physical mechanisms (e.g., Patruno et al. 2016; Cúneo et al. 2020; Alabarta et al. 2022; Saikia et al. 2023). During the decay, the small corona presents a feedback fraction similar to that during the rise and the reflare, while the large corona shows a lower feedback fraction, ranging from ~ 0 to ~ 0.3 . On the other hand, the sizes of both coronae are an order of magnitude smaller. This suggests that the geometry of the small corona is similar to that in the other two phases of the outburst, while the large corona is smaller and vertically extended. In all cases, the temperature of the seed photon of the large corona, kT_{s2} , is lower than the temperature of the inner part of the accretion disc, kT_{in} , suggesting that the large corona is illuminated by more external parts of the accretion disc, while the inner parts of the disc illuminate the small corona. In addition to this, the fact that $\eta_{int,1} \sim 0.03$ during the rise and reflare and $\eta_{int,1} \sim 0.15$ during the decay suggests that the disc is more truncated during the rise of the outburst and the reflare than during the outburst decay.

Taking into account the low values of $\eta_{int,2}$ from our fits, an alternative scenario for the large corona during the decay of the outburst would be the following: Kylafis & Reig (2024, Fig. 10) showed that only $\sim 1 - 10\%$ of the photons that escape at heights of $10^1 - 10^3 R_g$ out of an outflowing corona of radius

$100 R_g$ at the base, and a Lorentz factor of 2.24, return to the disc. Assuming that L_2 in our fits represents the height at which the photons escape the outflowing corona, both the L_2 and $\eta_{int,2}$ values we found during the decay of the outburst ($L_2 \sim 45 - 3000 R_g$ and $\eta_{int,2} \sim 0.05$, respectively) are consistent with the results of Kylafis & Reig (2024). Therefore, the large corona could be outflowing material (e.g., Giannios et al. 2004; Kylafis et al. 2008; Reig et al. 2018; Reig & Kylafis 2021; Kylafis & Reig 2024) and references therein.

Our results can be compared with those obtained with models of the family of ν KOMPETH for type-C QPOs observed in other BH LMXBs (García et al. 2022; Bellavita et al. 2022; Zhang et al. 2022; Rawat et al. 2023; Rout et al. 2023; Ma et al. 2023). García et al. (2022) and Bellavita et al. (2022) fitted the fractional rms and phase lag spectra of the type-C QPO detected in GRS 1915+105 during the HIMS with a single-corona model. García et al. (2022) considered a blackbody as the seed photon source of the corona, while Bellavita et al. (2022), on the other hand, used a disk blackbody. Both studies obtained a corona with a size of $L \sim 10^3 - 10^4$ km, $\eta < 0.2 - 0.3$ and $kT_s < 0.2$ keV, for QPO frequencies lower than 1.8 Hz (those consistent with the frequencies of the type-C QPO in MAXI J1348-630). Due to the relatively large size and low feedback, they interpreted it as a vertically extended corona with a jet-like structure.

Zhang et al. (2022) and Rawat et al. (2023) also modelled the fractional rms amplitude and phase lag spectra of the type-C QPO observed in MAXI J1535-571 with ν KOMPETH. Using, respectively, *HXMT* and *NICER* data, these authors found a corona whose size decreases from $\sim 10^4$ km to $\sim 10^3$ km as the

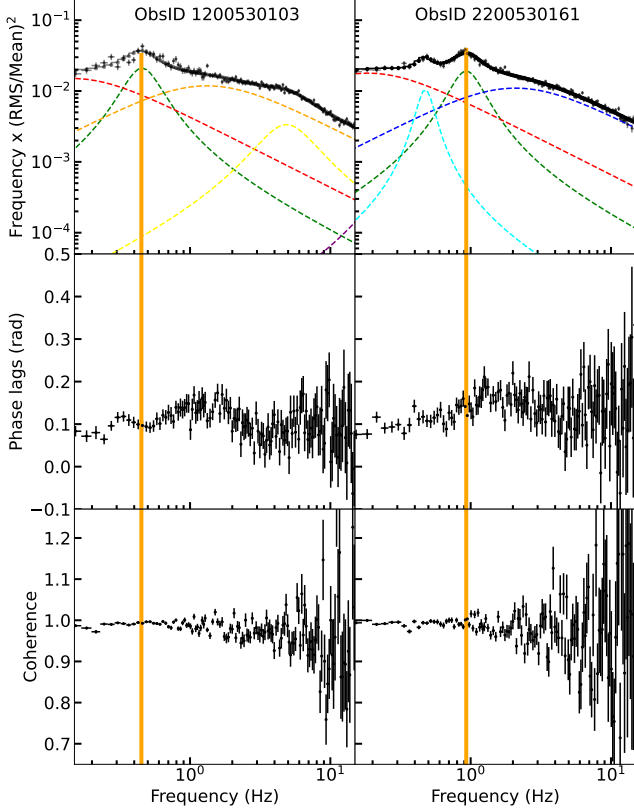


Figure 6. From top to bottom: PDS, phase lag and coherence vs frequency of the observations of MAXI J1348–630 showing type-C QPOs during the rise of the main outburst (left column) and flare (right column). The reference and subject bands are, respectively, 0.5–2.0 keV and 2.0–10.0 keV. Dashed lines represent the Lorentzians fitting the PDS. Green Lorentzian represents the type-C QPO, and the orange line marks the QPO frequency. Colours and symbols are as defined in the previous figure.

QPO frequency increases from $\nu_0 \sim 1.8$ Hz to $\nu_0 \sim 2.7$ Hz. The feedback fraction ranged between ~ 0.6 and ~ 0.8 , meaning that a 10%–25% of the fraction of the corona flux returned to the disc. Because of this and the simultaneous behaviour of the source in radio frequencies, these authors suggested a geometry in which there is a small corona in the inner parts of the system and a larger corona vertically extended consistent with the jet.

Rout et al. (2023), on the other hand, studied the geometry of the corona of GRO J1655–40 fitting the type-B and type-C QPOs that were detected simultaneously during the 2005 outburst of the system in the so-called ultraluminous state. These authors fitted the spectrum of the source and the fractional rms and phase lag spectra of both QPOs simultaneously with a single comptonisation region. Their results indicate that the type-C QPO comes from a corona with a size of $L \sim 10^3$ km and a feedback fraction of ~ 0.6 . These values suggested a horizontally extended corona covering partially the inner parts of the accretion disc.

Ma et al. (2023) studied the transition from type-C to type-B QPOs in MAXI J1820+070 during, respectively, the HIMS and the SIMS. Both QPOs were fitted with `vkDUALDK`, the model used in this study. For the type-C QPO, they found a small corona of $L_1 \sim 74$ km and an $\eta_1 \sim 0.5$, and a large corona of $L_2 \sim 10^4$ km and $\eta_2 \sim 1.0$. These parameters suggested a small corona located at the inner parts of the system and a large corona extending horizontally and covering the accretion disc, similar to that in GRO J1655–40.

Except in GRO J1655–40, the geometry of the corona in the above sources was studied during the HIMS. Comparing the results of MAXI J1348–630 during the HIMS, we found similar results to those presented above. The small corona of MAXI J1348–630 in the first observation of the decay of the main outburst is consistent with that of MAXI J1820+070, both in size and feedback. After that, the corona of MAXI J1348–630 increases in size. Regarding the large corona, both sources showed an $L_2 \sim 10^3$ km, but while the feedback fraction in MAXI J1820+070 was ~ 1.0 , in MAXI J1348–630 $\eta_2 < 0.4$. While the interpretation of Ma et al. (2023) was that the large corona extended horizontally in MAXI J1820+070, we interpreted it as extending vertically in MAXI J1348–630 due to the low feedback and the similar behaviour of the radio flux. The geometry of the large corona is more consistent with that of GRS 1915+105 presented in García et al. (2022) and Bellavita et al. (2022). The values of the corona in both GRO J1655–40 and MAXI J1535–571 are similar to those of the small corona of MAXI J1348–630, although in MAXI J1535–571 the corona is thought to be vertically extended. In MAXI J1348–630 during the LHS, the sizes of both coronae are higher than those observed in other sources. However, this is expected. As we show in Fig. 5 and Rawat et al. (2023) show in the top left panel of their Fig. 8, the size of the corona increases as the frequency of the QPO decreases. Then, the parameters we obtained are consistent with those described in the previous paragraph. We also note that independent results from X-ray polarization for Cyg X–1 in the LHS and Swift J1727.8–1613 in the HIMS show that the corona in the LHS is horizontally extended (Krawczynski et al. 2022; Ingram et al. 2024), as we found for MAXI J1348–630.

4.2. Other geometries for coronae

Previous works have studied the size and the evolution of the corona in BH LMXBs using different geometries (e.g., Ingram et al. 2009; Marcel et al. 2018b, 2019; Kara et al. 2019; Karpouzas et al. 2020; De Marco et al. 2021; Karpouzas et al. 2021; García et al. 2021; Marino et al. 2021; Wang et al. 2021a; Kawamura et al. 2022; Méndez et al. 2022; Wang et al. 2022; Zhang et al. 2023b). Assuming a lamppost geometry, Kara et al. (2019) interpreted the evolution of the soft broadband lags of MAXI J1820+070 and the constant width and

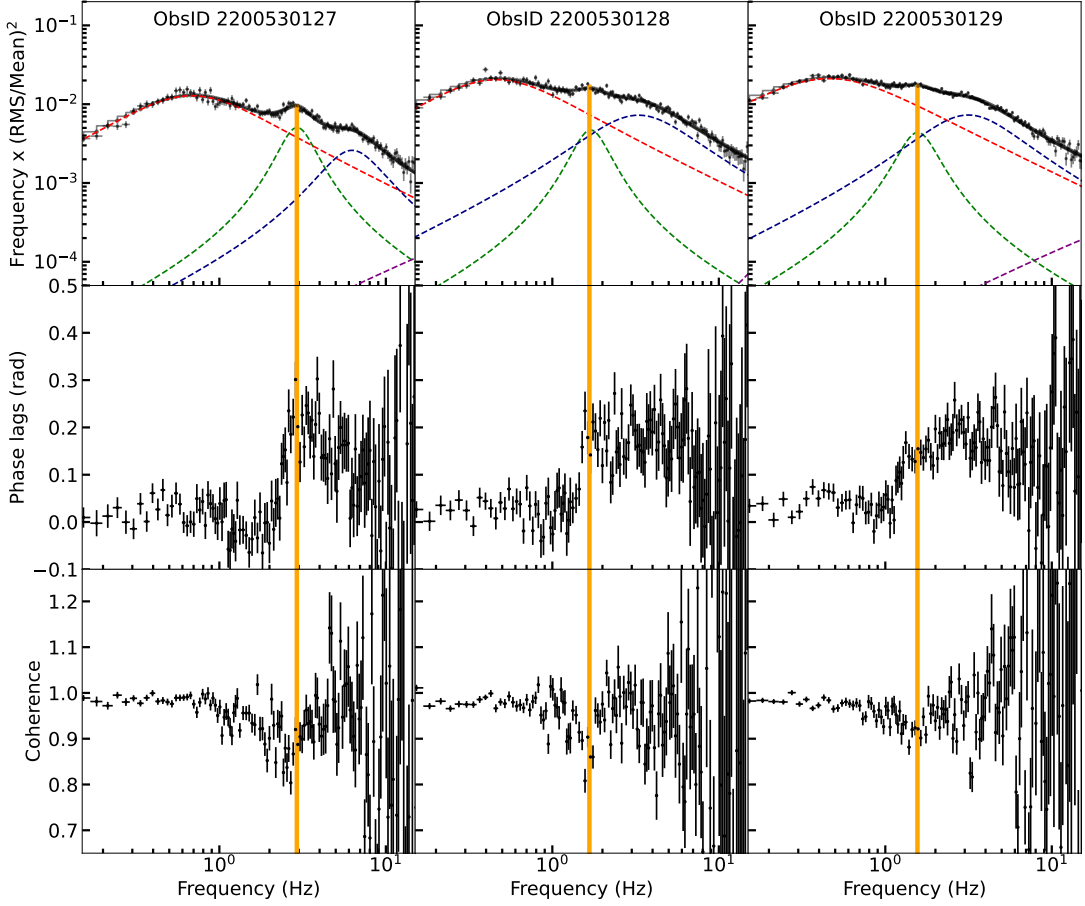


Figure 7. From top to bottom: PDS, phase lag vs frequency and coherence vs frequency of the observations of MAXI J1348–630 showing type-C QPOs during the decay of the main outburst. The reference and subject bands, colours and symbols are as defined in the previous figure.

centroid frequency of the Fe emission line as changes in the vertical size of the corona. In their interpretation the corona of MAXI J1820+070 contracts in the LHS; in a subsequent paper Wang et al. (2021a) proposed that the size of the corona increases again as the source evolves through the intermediate states. However, results from polarization studies suggest that the corona extends parallel to the accretion disc rather than vertically in the LHS (e.g., Krawczynski et al. 2022; Ingram et al. 2024), an interpretation that is also supported by the results of Ma et al. (2023) and this paper. Alternatively, De Marco et al. (2021) interpreted the evolution of the soft broadband lags of MAXI J1820+070 as a decrease of the inner disc radius instead of changes in the coronal geometry, which was assumed to remain constant. Assuming this is also true for MAXI J1348–630, Zhang et al. (2020a) showed that the normalization of the disc blackbody increases during the rise of the reflare and decreases during the decay. Since the normalization of the disc blackbody is proportional to the inner radius of the disc squared, changes in the normalization suggest that the radius of the disc is also evolving, which would support the interpretation of De Marco et al. (2021). However, our results fitting the ν KDUALDK strongly suggest that

the size of the Comptonization region changes. Alternatively, in the JED-SAD model (Ferreira 1997; Ferreira et al. 2006; Petrucci et al. 2008; Marcel et al. 2018a,b, 2019, 2020, 2022), the corona is thought to be a jet-emitting disc (JED) linked to the standard accretion disc (SAD) through a transition radius (r_j). In Marcel et al. (2020), the frequency of the type-C QPO is linked with r_j ($\nu_{QPO} \sim \nu_K(r_j)/q$), where ν_{QPO} and ν_K are, respectively, the QPO and the Keplerian frequency, and $q = 133 \pm 4$ is a scaling factor (Marcel et al. 2020). If we take the frequency of the type-C QPO of MAXI J1348–630, and assuming a $10M_\odot$ mass for the compact object of the system, we get a transition radius ranging from $2R_g$ to $7R_g$. This transition radius is between 1 and 3 orders of magnitude lower than the characteristic sizes for both the coronae we inferred from the rms and phase-lag spectra of the type-C QPO of MAXI J1348–630.

4.3. Evolution of the coronae during the whole outburst and reflare of MAXI J1348–630

Focusing on MAXI J1348–630, the geometry of its coronae has also been studied by the analysis of the radiative properties of the type-B and type-A QPOs (Zhang et al. 2021;

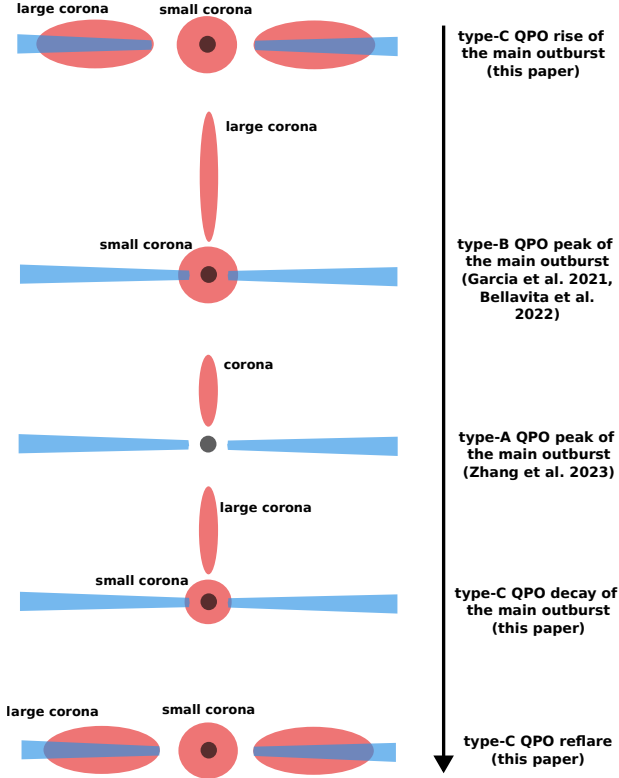


Figure 8. Schematic representation of the evolution of the coronae during the main outburst and the reflare of MAXI J1348–630 through the study of the type-A, -B and -C QPOs.

García et al. 2021; Bellavita et al. 2022; Zhang et al. 2023a). By carrying out a spectral-timing study of the fast appearance/disappearance of the type-B QPO, Zhang et al. (2021) found that, when the type-B QPO is present in the PDS of the system, an increase in the Comptonization emission is detected. This increase can be well-fitted with an extra Comptonization component in the energy spectrum. Considering that this extra component only appears simultaneously with the type-B QPO, Zhang et al. (2021) related it to the jet of the system. Independently, García et al. (2021) and Bellavita et al. (2022) described the fractional rms and phase lag spectra of the type-B QPO by a model consisting of two physically connected coronae: a small and horizontally extended corona and a large one that is vertically extended. Both these authors used the version of the time-dependent Comptonization model for two coronae. García et al. (2021) used a blackbody component as a seed photon source and found a small corona with a size of $L_1 \sim 10^3$ km and feedback fraction of $\eta_1 \sim 0.2$ and a large corona with $L_2 \sim 10^4$ km and $\eta_2 \sim 0.80$. Bellavita et al. (2022) used a disc-blackbody component as a

seed photon source. In this case, the size of the large corona was estimated to be $L_2 \sim 13400$ km with a relatively low $\eta_2 \sim 0.35$. The small corona, on the other hand, presents a size of $L_1 \sim 160$ km and a feedback fraction of $\eta_1 > 0.9$. They related the large corona with the emission of the base of the discrete jet that was being developed at the same time (Carotenuto et al. 2022). Zhang et al. (2023a), on the other hand, jointly fitted the time-average energy spectrum of the type-A QPO with the model `vkompthdk`, that assumes a single corona with a disc blackbody as a seed photon source. They got a corona with a characteristic size of ~ 2300 km and a $kT_s \sim 0.4$ keV lower than kT_{in} . Due to the latter, they suggested a vertically extended geometry for the corona, similar to the one derived from the type-B QPO, but on a smaller scale.

This paper completes the analysis of the *NICER* data of the 2019 outburst of MAXI J1348–630 with the family of `vkompth` models to fit the fractional rms and phase-lag spectra of the QPOs observed in this source. Therefore, we can compile the results derived from fitting the three different types of QPO and present the evolution of the properties of the coronae through the outbursts and the first reflare.

The first two observations in MAXI J1348–630 (MJD 58511 and MJD 58512) with a QPO occur in the LHS during the rise of the main outburst and correspond to a type-C QPO of frequencies ~ 0.4 Hz and ~ 0.5 Hz. From the fits, we found two coronae horizontally extended: one small of $L_1 \sim 6300$ km that shrinks to $L_1 \sim 760$ km and a large corona that increases from $L_2 \sim 39200$ km to $L_2 \sim 55000$ km. In these two observations, the feedback fraction of the two regions is $\eta_1 \sim 0.7$ and $\eta_2 < 1.0$. Later, during seven days (from MJD 58522 to MJD 58540, see Belloni et al. 2020, for the list of dates) a type-B QPO was observed in the PDS of MAXI J1348–630, and the source entered the SIMS. The small corona is still horizontally extended with a size of $L_1 \sim 150$ km and $\eta_1 > 0.9$, and the large corona is now vertically extended with a size of ~ 12200 km and $\eta_2 > 0.25$. Due to the behaviour of the system, the vertical corona could be associated as the base of the jet if the corona feeds the jet. A few days later (from MJD 58543 to MJD 58539, see Zhang et al. 2023a, for the list of dates), when the type-A QPO was detected, the source was already in the HSS. Fitting the time-average spectrum of the source and the rms and phase-lag spectra of the QPO with a single corona, a vertically extended corona of ~ 2300 km and a feedback fraction of ~ 0.5 was obtained. We can identify this as the large corona of the type-C and type-B QPOs that shrank in the HSS. When the decay of the outburst started, the source entered the HIMS again, and a type-C QPO was detected (from MJD 58603 to MJD 58606). The small corona, in this case, started with a size of $L_1 \sim 45$ km, then increased to $L_1 \sim 1000$ km and

finally decreased to $L_1 \sim 400$ km, with a feedback fraction ranging from ~ 0.5 to ~ 0.8 . The large corona, on the other hand, started with a size of $L_2 \sim 600$ km, then increased to $L_2 \sim 44000$ km and finally decreased to $L_2 \sim 7000$ km, with a feedback fraction always lower than ~ 0.3 . In MJD 58602 and MJD 58603, a sudden increase in the radio flux was detected, followed by a decrease in MJD 58607 (Carotenuto et al. 2021). Because of this and the low η_2 , we tentatively suggest that the large corona is associated with the base of the newly formed compact jet. Finally, during the reflare (see Table. 1), the size of the small corona, L_1 , ranges between ~ 700 km and ~ 3500 km with a feedback fraction between ~ 0.7 and ~ 1.0 . Extending the interpretation, the large corona became horizontally extended again, with sizes between ~ 14500 km to ~ 63000 km, with η_2 always higher than 0.5. A schematic representation of the evolution of the coronae is shown in Fig. 8.

4.4. Implications of the drop in coherence at the QPO frequency

König et al. (2024) found a sudden increase of the time lags and a sharp drop of the coherence as a function of Fourier frequency happening at frequencies between two broad Lorentzians in the PDS in some observations of Cyg X-1, MAXI J1820+070, MAXI J1348-630 and AT 2019wey (see, e.g., their Fig. 17). In MAXI J1820+070 and MAXI J1348-630, both the increase of the lags and the drop in the coherence only appeared in the soft-to-hard transition happening during the decay of the outburst, and the frequency at which they are observed, increases as the source gets softer. Using a new analysis method, Méndez et al. (2024) fitted the PDS and the CS with the same Lorentzian components and found that at the same frequency, a narrow Lorentzian appears in the CS but not in the PDS, being more significant in the Imaginary than in the Real part of the CS. Due to its large Imaginary part, Méndez et al. (2024) called it “Imaginary QPO”. This feature was interpreted as a potential beat between the two broad Lorentzians by König et al. (2024), whereas Méndez et al. (2024) argued that Imaginary QPOs represent an independent phenomenon.

In the case of MAXI J1348-630, the cliff in the phase lags and the drop in the coherence function occur at the same frequency as that of the type-C QPO. Contrary to the cases of Cyg X-1 and MAXI J1820+070, the features in the lags and coherence are consistent with a significant Lorentzian in the PDS. This is the first time that the cliff in the lags and the drop in coherence are linked to a component observed in the PDS and, in particular, to a type-C QPO. Moreover, our result also suggests a potential relation between type-C and Imaginary QPOs, although a link between the latter and other types of QPOs cannot be ruled out (Bellavita et al. 2024, in preparation).

This particular behaviour of the phase lags and the coherence function of MAXI J1348-630 is only observed in the decay of an outburst during the soft-to-hard transition. This result is consistent with the Imaginary QPO of MAXI J1820+070 (Méndez et al. 2024; König et al. 2024, Bellavita et al. 2024, in preparation). The energy dependence of the phase lags of the type-C QPO during this phase of the outburst of MAXI J1348-630 (Fig. 3) is very similar to that of the Imaginary QPO of MAXI J1820+070 (Fig. 6 of Bellavita et al. 2024, in preparation). Both show large phase lag variations, of ~ 0.8 rad and ~ 1.5 rad, respectively, between soft and hard energies. In terms of the contribution of the Imaginary and Real parts of the CS, these larger lags reflect the fact that the cross vector has a large Imaginary part at the QPO frequency (see the definition of the lags in Section 2.3). The magnitude of the phase lag of the type-C QPO in the LHS of MAXI J1348-630, on the other hand, is smaller (between ~ 0.2 rad and ~ 0.4 rad, see left and right panels of Fig. 3), meaning that, compared to the Real part, the Imaginary part of the CS is smaller than that in the HIMS.

On the basis of the above, two questions arise: why do the cliff in the lags and the drop in coherence only appear in the soft-to-hard transition and not in the LHS? And can we relate the behaviour of the lags and coherence to the evolution of the corona? We can conjecture about these questions under the light of the radiative properties of the type-C QPO of MAXI J1348-630. Both in Alabarta et al. (2022) and this paper, we showed that the fractional rms amplitude and the phase lags of the type-C QPO are consistent with being produced by oscillations in the properties of the corona. We also found evidence that the geometry of the corona of MAXI J1348-630 changes through the outburst, similarly to other sources (e.g., Kara et al. 2019; Wang et al. 2021b; García et al. 2022; Méndez et al. 2022; Rout et al. 2023; Ma et al. 2023). When the source is in the LHS, the Comptonization region is described by two coronae: a small and a large one, both with relatively high feedback ($\eta_{1,2} > 0.5$). Because of this, we interpreted them as being extended horizontally in the direction of the accretion disc. Since the feedback measures the fraction of the flux of the disc that originates from photons coming from the corona, a high feedback fraction implies a strong interaction between the corona and the accretion disc. This strong interaction can explain the high coherence (~ 1) that we observe at the frequency of the type-C QPO in Fig. 6. On the contrary, the Comptonization region during the decay of the outburst, while the system is in the HIMS, is described by a small corona with similar properties as in the LHS and a large corona with a very low feedback fraction ($\eta_2 < 0.3$) that is interpreted to be vertically extended. This very low feedback implies that the large corona does not interact as much with the accretion disc as in the LHS. This weaker interaction between the large corona and the accretion disc could

explain the drop in the coherence observed at the frequency of the type-C QPO during the decay of the outburst. Moreover, the different geometry of the large corona in the decay with respect to that in the LHS would explain why the drop in coherence is only observed during the state transition and not in the LHS.

5. SUMMARY AND CONCLUSIONS

In this work, we show that the rms and lag spectra of the type-C QPO detected in MAXI J1348–630 with *NICER* during its 2019 outburst and reflare can be explained in terms of two independent but physically coupled coronae. Indeed, we can successfully fit jointly the time-averaged spectrum of the source and the rms and phase-lag spectra of the QPO with the time-dependent Comptonization model *VKDUALDK* (Karpouzas et al. 2020; Bellavita et al. 2022). Moreover, we found a sudden increase of the phase lag frequency spectrum (the “cliff”) and a drop of the coherence function at the same frequency of the type-C QPO during the decay of the outburst. This is the first time that this cliff in the lags and the corresponding sharp drop in the coherence function are directly connected to a type-C QPO in the PDS. We explain this cliff in the lag and drop in the coherence in terms of the geometry of the coronae of MAXI J1348–630. Our main conclusions are the following:

1. The fractional rms and phase lag spectra of the QPO can be fitted with two physically coupled coronae: one small and one large corona.
2. During the rise of the main outburst and the reflare, both in the LHS, the characteristic size of the small corona is $\sim 10^2\text{--}10^3$ km with a feedback-fraction of >0.6 . The size of the large corona, on the other hand, is $\sim 10^4$ km, and this corona also presents a high feedback fraction >0.6 . Due to the high feedback fractions, the coronae are interpreted as being horizontally extended over the accretion disc.
3. During the decay of the outburst, when the system is in the HIMS, the size of the small corona is $L_1 \sim 10^1\text{--}10^3$

km and the feedback fraction is similar to that during the rise and the reflare. The size of the large corona is $\sim 10^2\text{--}10^4$ km, with a lower feedback fraction ($\eta_2 < 0.3$). Due to the values of η_2 and the evolution of the radio flux during these observations, we interpreted the large corona as being vertically extended.

4. König et al. (2024) found a sudden increase in the phase lag frequency spectrum (the cliff) and a drop in the coherence function in one observation during the decay of the outburst of MAXI J1348–630. We found these features in the observations of the decay showing the type-C QPO but not in those with the QPO in the LHS in the rise and the reflare. Moreover, the cliff in the lags and the drop of the coherence occur at the same frequency as the QPO in the PDS, suggesting that this signal is responsible for these features. We hypothesise that the drop in the coherence function occurs in the HIMS but not in the LHS because of the differences in the geometry of large corona in both spectral states.

ACKNOWLEDGEMENTS

This material is based upon work supported by Tamkeen under the NYU Abu Dhabi Research Institute grant CASS. This work is based on observations made by the *NICER* X-ray mission supported by NASA. This research has made use of data and software provided by the High Energy Astrophysics Science Archive Research Center (HEASARC), a service of the Astrophysics Science Division at NASA/GSFC and the High Energy Astrophysics Division of the Smithsonian Astrophysical Observatory. The authors acknowledge Dr. Sandeep Rout for the discussion about the geometry of the coronae. MM acknowledges the research programme Athena with project number 184.034.002, which is (partly) financed by the Dutch Research Council (NWO). FG is a CONICET researcher. FG acknowledges support by PIBAA 1275 and PIP 0113 (CONICET). YZ acknowledges support from the Dutch Research Council (NWO) Rubicon Fellowship, file no. 019.231EN.021.

REFERENCES

- Alabarta, K., Méndez, M., García, F., et al. 2022, *MNRAS*, 514, 2839, doi: [10.1093/mnras/stac1533](https://doi.org/10.1093/mnras/stac1533)
- Altamirano, D., Belloni, T., Linares, M., et al. 2011, *ApJL*, 742, L17, doi: [10.1088/2041-8205/742/2/L17](https://doi.org/10.1088/2041-8205/742/2/L17)
- Arévalo, P., & Uttley, P. 2006, *MNRAS*, 367, 801, doi: [10.1111/j.1365-2966.2006.09989.x](https://doi.org/10.1111/j.1365-2966.2006.09989.x)
- Arnaud, K. A. 1996, in *Astronomical Society of the Pacific Conference Series*, Vol. 101, *Astronomical Data Analysis Software and Systems V*, ed. G. H. Jacoby & J. Barnes, 17
- Axelsson, M., & Done, C. 2016, *MNRAS*, 458, 1778, doi: [10.1093/mnras/stw464](https://doi.org/10.1093/mnras/stw464)
- Bellavita, C., García, F., Méndez, M., & Karpouzas, K. 2022, *MNRAS*, 515, 2099, doi: [10.1093/mnras/stac1922](https://doi.org/10.1093/mnras/stac1922)

- Belloni, T., ed. 2010a, *Lecture Notes in Physics*, Berlin Springer Verlag, Vol. 794, The Jet Paradigm, doi: [10.1007/978-3-540-76937-8](https://doi.org/10.1007/978-3-540-76937-8)
- Belloni, T., Homan, J., Casella, P., et al. 2005, *A&A*, 440, 207, doi: [10.1051/0004-6361:20042457](https://doi.org/10.1051/0004-6361:20042457)
- Belloni, T., Psaltis, D., & van der Klis, M. 2002, *ApJ*, 572, 392, doi: [10.1086/340290](https://doi.org/10.1086/340290)
- Belloni, T. M. 2010b, in *The Jet Paradigm, Lecture Notes in Physics*, Volume 794. ISBN 978-3-540-76936-1. Springer-Verlag Berlin Heidelberg, 2010, p. 53, ed. T. Belloni, Vol. 794, 53, doi: [10.1007/978-3-540-76937-8_3](https://doi.org/10.1007/978-3-540-76937-8_3)
- Belloni, T. M., Motta, S. E., & Muñoz-Darias, T. 2011, *Bulletin of the Astronomical Society of India*, 39, 409. <https://arxiv.org/abs/1109.3388>
- Belloni, T. M., Zhang, L., Kylafis, N. D., Reig, P., & Altamirano, D. 2020, *MNRAS*, 496, 4366, doi: [10.1093/mnras/staa1843](https://doi.org/10.1093/mnras/staa1843)
- Callanan, P. J., Garcia, M. R., McClintock, J. E., et al. 1995, *ApJ*, 441, 786, doi: [10.1086/175402](https://doi.org/10.1086/175402)
- Cangemi, F., Rodriguez, J., Belloni, T., Clavel, M., & Grinberg, V. 2019, *The Astronomer's Telegram*, 12457, 1
- Carotenuto, F., Tetarenko, A. J., & Corbel, S. 2022, *MNRAS*, 511, 4826, doi: [10.1093/mnras/stac329](https://doi.org/10.1093/mnras/stac329)
- Carotenuto, F., Corbel, S., Tremou, E., et al. 2021, *MNRAS*, 504, 444, doi: [10.1093/mnras/stab864](https://doi.org/10.1093/mnras/stab864)
- Casella, P., Belloni, T., Homan, J., & Stella, L. 2004, *A&A*, 426, 587, doi: [10.1051/0004-6361:20041231](https://doi.org/10.1051/0004-6361:20041231)
- Casella, P., Belloni, T., & Stella, L. 2005, *ApJ*, 629, 403, doi: [10.1086/431174](https://doi.org/10.1086/431174)
- Chen, W., Shrader, C. R., & Livio, M. 1997, *ApJ*, 491, 312, doi: [10.1086/304921](https://doi.org/10.1086/304921)
- Cui, W., Zhang, S. N., & Chen, W. 2000, *ApJL*, 531, L45, doi: [10.1086/312520](https://doi.org/10.1086/312520)
- Cui, W., Zhang, S. N., Focke, W., & Swank, J. H. 1997, *ApJ*, 484, 383, doi: [10.1086/304341](https://doi.org/10.1086/304341)
- Cúneo, V. A., Alabarta, K., Zhang, L., et al. 2020, *MNRAS*, 496, 1001, doi: [10.1093/mnras/staa1606](https://doi.org/10.1093/mnras/staa1606)
- Dauser, T., Garcia, J., Parker, M. L., Fabian, A. C., & Wilms, J. 2014, *MNRAS*, 444, L100, doi: [10.1093/mnras/slu125](https://doi.org/10.1093/mnras/slu125)
- De Marco, B., Ponti, G., Muñoz-Darias, T., & Nandra, K. 2015, *ApJ*, 814, 50, doi: [10.1088/0004-637X/814/1/50](https://doi.org/10.1088/0004-637X/814/1/50)
- De Marco, B., Zdziarski, A. A., Ponti, G., et al. 2021, *arXiv e-prints*, arXiv:2102.07811. <https://arxiv.org/abs/2102.07811>
- D'Elia, V., Lien, A. Y., & Page, K. L. 2019a, *GRB Coordinates Network*, 23795, 1
- . 2019b, *GRB Coordinates Network*, 23796, 1
- Denisenko, D., Denisenko, I., Evtushenko, M., et al. 2019, *The Astronomer's Telegram*, 12430, 1
- Fabian, A. C., Rees, M. J., Stella, L., & White, N. E. 1989, *MNRAS*, 238, 729, doi: [10.1093/mnras/238.3.729](https://doi.org/10.1093/mnras/238.3.729)
- Ferreira, J. 1997, *A&A*, 319, 340, doi: [10.48550/arXiv.astro-ph/9607057](https://doi.org/10.48550/arXiv.astro-ph/9607057)
- Ferreira, J., Petrucci, P. O., Henri, G., Saugé, L., & Pelletier, G. 2006, *A&A*, 447, 813, doi: [10.1051/0004-6361:20052689](https://doi.org/10.1051/0004-6361:20052689)
- García, F., Karpouzas, K., Méndez, M., et al. 2022, *MNRAS*, 513, 4196, doi: [10.1093/mnras/stac1202](https://doi.org/10.1093/mnras/stac1202)
- García, F., Méndez, M., Karpouzas, K., et al. 2021, *MNRAS*, 501, 3173, doi: [10.1093/mnras/staa3944](https://doi.org/10.1093/mnras/staa3944)
- García, J., Dauser, T., Lohfink, A., et al. 2014, *ApJ*, 782, 76, doi: [10.1088/0004-637X/782/2/76](https://doi.org/10.1088/0004-637X/782/2/76)
- Giannios, D., Kylafis, N. D., & Psaltis, D. 2004, *A&A*, 425, 163, doi: [10.1051/0004-6361:20041002](https://doi.org/10.1051/0004-6361:20041002)
- Homan, J., & Belloni, T. 2005, *Ap&SS*, 300, 107, doi: [10.1007/s10509-005-1197-4](https://doi.org/10.1007/s10509-005-1197-4)
- Ingram, A., Done, C., & Fragile, P. C. 2009, *MNRAS*, 397, L101, doi: [10.1111/j.1745-3933.2009.00693.x](https://doi.org/10.1111/j.1745-3933.2009.00693.x)
- Ingram, A., Mastroserio, G., Dauser, T., et al. 2019, *MNRAS*, 488, 324, doi: [10.1093/mnras/stz1720](https://doi.org/10.1093/mnras/stz1720)
- Ingram, A., & Motta, S. 2020, *arXiv e-prints*, arXiv:2001.08758. <https://arxiv.org/abs/2001.08758>
- Ingram, A., & van der Klis, M. 2013, *MNRAS*, 434, 1476, doi: [10.1093/mnras/stt1107](https://doi.org/10.1093/mnras/stt1107)
- Ingram, A., Bollemeijer, N., Veledina, A., et al. 2024, *ApJ*, 968, 76, doi: [10.3847/1538-4357/ad3faf](https://doi.org/10.3847/1538-4357/ad3faf)
- Ji, J. F., Zhang, S. N., Qu, J. L., & Li, T. P. 2003, *ApJL*, 584, L23, doi: [10.1086/368269](https://doi.org/10.1086/368269)
- Jithesh, V., Maqbool, B., Misra, R., et al. 2019, *ApJ*, 887, 101, doi: [10.3847/1538-4357/ab4f6a](https://doi.org/10.3847/1538-4357/ab4f6a)
- Jonker, P. G., Miller-Jones, J. C. A., Homan, J., et al. 2012, *MNRAS*, 423, 3308, doi: [10.1111/j.1365-2966.2012.21116.x](https://doi.org/10.1111/j.1365-2966.2012.21116.x)
- Kara, E., Steiner, J. F., Fabian, A. C., et al. 2019, *Nature*, 565, 198, doi: [10.1038/s41586-018-0803-x](https://doi.org/10.1038/s41586-018-0803-x)
- Karpouzas, K., Méndez, M., García, F., et al. 2021, *MNRAS*, 503, 5522, doi: [10.1093/mnras/stab827](https://doi.org/10.1093/mnras/stab827)
- Karpouzas, K., Méndez, M., Ribeiro, E. r. M., et al. 2020, *MNRAS*, 492, 1399, doi: [10.1093/mnras/stz3502](https://doi.org/10.1093/mnras/stz3502)
- Kawamura, T., Axelsson, M., Done, C., & Takahashi, T. 2022, *MNRAS*, 511, 536, doi: [10.1093/mnras/stac045](https://doi.org/10.1093/mnras/stac045)
- Kompaneets, A. S. 1957, *Soviet Journal of Experimental and Theoretical Physics*, 4, 730
- König, O., Mastroserio, G., Dauser, T., et al. 2024, *arXiv e-prints*, arXiv:2405.07754, doi: [10.48550/arXiv.2405.07754](https://doi.org/10.48550/arXiv.2405.07754)
- Krawczynski, H., Muleri, F., Dovčiak, M., et al. 2022, *Science*, 378, 650, doi: [10.1126/science.add5399](https://doi.org/10.1126/science.add5399)
- Kumar, N., & Misra, R. 2014, *MNRAS*, 445, 2818, doi: [10.1093/mnras/stu1946](https://doi.org/10.1093/mnras/stu1946)
- Kylafis, N., & Reig, P. 2024, *arXiv e-prints*, arXiv:2407.05729, doi: [10.48550/arXiv.2407.05729](https://doi.org/10.48550/arXiv.2407.05729)
- Kylafis, N. D., Papadakis, I. E., Reig, P., Giannios, D., & Pooley, G. G. 2008, *A&A*, 489, 481, doi: [10.1051/0004-6361:20079159](https://doi.org/10.1051/0004-6361:20079159)

- Kylafis, N. D., & Reig, P. 2018, *A&A*, 614, L5, doi: [10.1051/0004-6361/201833339](https://doi.org/10.1051/0004-6361/201833339)
- Kylafis, N. D., Reig, P., & Tsouros, A. 2023, *A&A*, 679, A81, doi: [10.1051/0004-6361/202346379](https://doi.org/10.1051/0004-6361/202346379)
- Lee, H. C., Misra, R., & Taam, R. E. 2001, *ApJL*, 549, L229, doi: [10.1086/319171](https://doi.org/10.1086/319171)
- Lucchini, M., Mastroserio, G., Wang, J., et al. 2023, *ApJ*, 951, 19, doi: [10.3847/1538-4357/acd24f](https://doi.org/10.3847/1538-4357/acd24f)
- Ludlam, R. M., Miller, J. M., Arzoumanian, Z., et al. 2018, *ApJL*, 858, L5, doi: [10.3847/2041-8213/aabee6](https://doi.org/10.3847/2041-8213/aabee6)
- Ma, R., Méndez, M., García, F., et al. 2023, *MNRAS*, 525, 854, doi: [10.1093/mnras/stad2284](https://doi.org/10.1093/mnras/stad2284)
- Ma, X., Tao, L., Zhang, S.-N., et al. 2021, *Nature Astronomy*, 5, 94, doi: [10.1038/s41550-020-1192-2](https://doi.org/10.1038/s41550-020-1192-2)
- Marcel, G., Ferreira, J., Petrucci, P. O., et al. 2018a, *A&A*, 615, A57, doi: [10.1051/0004-6361/201732069](https://doi.org/10.1051/0004-6361/201732069)
- . 2018b, *A&A*, 617, A46, doi: [10.1051/0004-6361/201833124](https://doi.org/10.1051/0004-6361/201833124)
- Marcel, G., Ferreira, J., Clavel, M., et al. 2019, *A&A*, 626, A115, doi: [10.1051/0004-6361/201935060](https://doi.org/10.1051/0004-6361/201935060)
- Marcel, G., Cangemi, F., Rodriguez, J., et al. 2020, *A&A*, 640, A18, doi: [10.1051/0004-6361/202037539](https://doi.org/10.1051/0004-6361/202037539)
- Marcel, G., Ferreira, J., Petrucci, P. O., et al. 2022, *A&A*, 659, A194, doi: [10.1051/0004-6361/202141375](https://doi.org/10.1051/0004-6361/202141375)
- Marino, A., Barnier, S., Petrucci, P. O., et al. 2021, *A&A*, 656, A63, doi: [10.1051/0004-6361/202141146](https://doi.org/10.1051/0004-6361/202141146)
- Markoff, S., Nowak, M. A., & Wilms, J. 2005, *ApJ*, 635, 1203, doi: [10.1086/497628](https://doi.org/10.1086/497628)
- Méndez, M., Karpouzias, K., García, F., et al. 2022, *Nature Astronomy*, 6, 577, doi: [10.1038/s41550-022-01617-y](https://doi.org/10.1038/s41550-022-01617-y)
- Méndez, M., Peirano, V., García, F., et al. 2024, *MNRAS*, 527, 9405, doi: [10.1093/mnras/stad3786](https://doi.org/10.1093/mnras/stad3786)
- Méndez, M., & van der Klis, M. 1997, *ApJ*, 479, 926, doi: [10.1086/303914](https://doi.org/10.1086/303914)
- Miller, J. M., Gendreau, K., Ludlam, R. M., et al. 2018, *ApJL*, 860, L28, doi: [10.3847/2041-8213/aacc61](https://doi.org/10.3847/2041-8213/aacc61)
- Miyamoto, S., Kitamoto, S., Mitsuda, K., & Dotani, T. 1988, *Nature*, 336, 450, doi: [10.1038/336450a0](https://doi.org/10.1038/336450a0)
- Motta, S. E. 2016, *Astronomische Nachrichten*, 337, 398, doi: [10.1002/asna.201612320](https://doi.org/10.1002/asna.201612320)
- Muñoz-Darias, T., Motta, S., & Belloni, T. M. 2011, *MNRAS*, 410, 679, doi: [10.1111/j.1365-2966.2010.17476.x](https://doi.org/10.1111/j.1365-2966.2010.17476.x)
- Muñoz-Darias, T., Motta, S., Pawar, D., et al. 2010, *MNRAS*, 404, L94, doi: [10.1111/j.1745-3933.2010.00842.x](https://doi.org/10.1111/j.1745-3933.2010.00842.x)
- Nobili, L., Turolla, R., Zampieri, L., & Belloni, T. 2000, *ApJL*, 538, L137, doi: [10.1086/312810](https://doi.org/10.1086/312810)
- Nowak, M. A. 2000, *MNRAS*, 318, 361, doi: [10.1046/j.1365-8711.2000.03668.x](https://doi.org/10.1046/j.1365-8711.2000.03668.x)
- Nowak, M. A., Vaughan, B. A., Wilms, J., Dove, J. B., & Begelman, M. C. 1999, *ApJ*, 510, 874, doi: [10.1086/306610](https://doi.org/10.1086/306610)
- Pahari, M., Neilsen, J., Yadav, J. S., Misra, R., & Uttley, P. 2013, *ApJ*, 778, 136, doi: [10.1088/0004-637X/778/2/136](https://doi.org/10.1088/0004-637X/778/2/136)
- Patruno, A., Maitra, D., Curran, P. A., et al. 2016, *ApJ*, 817, 100, doi: [10.3847/0004-637X/817/2/100](https://doi.org/10.3847/0004-637X/817/2/100)
- Payne, D. G. 1980, *ApJ*, 237, 951, doi: [10.1086/157941](https://doi.org/10.1086/157941)
- Peirano, V., Méndez, M., García, F., & Belloni, T. 2023, *MNRAS*, 519, 1336, doi: [10.1093/mnras/stac3553](https://doi.org/10.1093/mnras/stac3553)
- Petrucci, P.-O., Ferreira, J., Henri, G., & Pelletier, G. 2008, *MNRAS*, 385, L88, doi: [10.1111/j.1745-3933.2008.00439.x](https://doi.org/10.1111/j.1745-3933.2008.00439.x)
- Plant, D. S., Fender, R. P., Ponti, G., Muñoz-Darias, T., & Coriat, M. 2014, *MNRAS*, 442, 1767, doi: [10.1093/mnras/stu867](https://doi.org/10.1093/mnras/stu867)
- Psaltis, D., Belloni, T., & van der Klis, M. 1999, *ApJ*, 520, 262, doi: [10.1086/307436](https://doi.org/10.1086/307436)
- Rawat, D., Méndez, M., García, F., et al. 2023, *MNRAS*, 520, 113, doi: [10.1093/mnras/stad126](https://doi.org/10.1093/mnras/stad126)
- Reig, P., Belloni, T., van der Klis, M., et al. 2000, arXiv e-prints, astro. <https://arxiv.org/abs/astro-ph/0001134>
- Reig, P., & Kylafis, N. D. 2021, *A&A*, 646, A112, doi: [10.1051/0004-6361/202039903](https://doi.org/10.1051/0004-6361/202039903)
- Reig, P., Kylafis, N. D., Papadakis, I. E., & Costado, M. T. 2018, *MNRAS*, 473, 4644, doi: [10.1093/mnras/stx2683](https://doi.org/10.1093/mnras/stx2683)
- Remillard, R., Levine, A. M., Morgan, E. H., Markwardt, C. B., & Swank, J. H. 2006, *The Astronomer's Telegram*, 714
- Remillard, R. A., & McClintock, J. E. 2006, *Annual Review of Astronomy and Astrophysics*, 44, 49, doi: [10.1146/annurev.astro.44.051905.092532](https://doi.org/10.1146/annurev.astro.44.051905.092532)
- Remillard, R. A., Loewenstein, M., Steiner, J. F., et al. 2022, *AJ*, 163, 130, doi: [10.3847/1538-3881/ac4ae6](https://doi.org/10.3847/1538-3881/ac4ae6)
- Reynolds, A. P., Parmar, A. N., Hakala, P. J., et al. 1999, *A&AS*, 134, 287, doi: [10.1051/aas:1999140](https://doi.org/10.1051/aas:1999140)
- Rodriguez, J., Corbel, S., Hannikainen, D. C., et al. 2004a, *ApJ*, 615, 416, doi: [10.1086/423978](https://doi.org/10.1086/423978)
- Rodriguez, J., Corbel, S., Kalemci, E., Tomsick, J. A., & Tagger, M. 2004b, *ApJ*, 612, 1018, doi: [10.1086/422672](https://doi.org/10.1086/422672)
- Rout, S. K., Méndez, M., & García, F. 2023, *MNRAS*, 525, 221, doi: [10.1093/mnras/stad2321](https://doi.org/10.1093/mnras/stad2321)
- Russell, D. M., Baglio, C. M., & Lewis, F. 2019a, *The Astronomer's Telegram*, 12439, 1
- Russell, T., Anderson, G., Miller-Jones, J., et al. 2019b, *The Astronomer's Telegram*, 12456, 1
- Saikia, P., Russell, D. M., Pirbhoy, S. F., et al. 2023, *ApJ*, 949, 104, doi: [10.3847/1538-4357/acc8cc](https://doi.org/10.3847/1538-4357/acc8cc)
- Sanna, A., Uttley, P., Altamirano, D., et al. 2019, *The Astronomer's Telegram*, 12447, 1
- Shakura, N. I., & Sunyaev, R. A. 1973, in *IAU Symposium*, Vol. 55, X- and Gamma-Ray Astronomy, ed. H. Bradt & R. Giacconi, 155
- Sobolewska, M. A., & Życki, P. T. 2006, *MNRAS*, 370, 405, doi: [10.1111/j.1365-2966.2006.10489.x](https://doi.org/10.1111/j.1365-2966.2006.10489.x)

- Tanaka, Y. 1989, in ESA Special Publication, Vol. 1, Two Topics in X-Ray Astronomy, Volume 1: X Ray Binaries. Volume 2: AGN and the X Ray Background, ed. J. Hunt & B. Battrock, 3
- Tominaga, M., Nakahira, S., Shidatsu, M., et al. 2020, *ApJL*, 899, L20, doi: [10.3847/2041-8213/abaaaa](https://doi.org/10.3847/2041-8213/abaaaa)
- Tomsick, J. A., & Kaaret, P. 2001, *ApJ*, 548, 401, doi: [10.1086/318683](https://doi.org/10.1086/318683)
- Uttley, P., Cackett, E. M., Fabian, A. C., Kara, E., & Wilkins, D. R. 2014, *A&A Rv*, 22, 72, doi: [10.1007/s00159-014-0072-0](https://doi.org/10.1007/s00159-014-0072-0)
- van der Klis, M. 1989, *ARA&A*, 27, 517, doi: [10.1146/annurev.aa.27.090189.002505](https://doi.org/10.1146/annurev.aa.27.090189.002505)
- . 1994, *ApJS*, 92, 511, doi: [10.1086/192006](https://doi.org/10.1086/192006)
- . 2000, *ARA&A*, 38, 717, doi: [10.1146/annurev.astro.38.1.717](https://doi.org/10.1146/annurev.astro.38.1.717)
- van der Klis, M., Swank, J., Zhang, W., et al. 1996, *IAUC*, 6319, 1
- Vaughan, B., van der Klis, M., Lewin, W. H. G., et al. 1994, *ApJ*, 421, 738, doi: [10.1086/173686](https://doi.org/10.1086/173686)
- Vaughan, B. A., & Nowak, M. A. 1997, *ApJL*, 474, L43, doi: [10.1086/310430](https://doi.org/10.1086/310430)
- Verner, D. A., Ferland, G. J., Korista, K. T., & Yakovlev, D. G. 1996, *ApJ*, 465, 487, doi: [10.1086/177435](https://doi.org/10.1086/177435)
- Wang, J., Mastroserio, G., Kara, E., et al. 2021a, *ApJL*, 910, L3, doi: [10.3847/2041-8213/abec79](https://doi.org/10.3847/2041-8213/abec79)
- Wang, J., Kara, E., Lucchini, M., et al. 2022, *ApJ*, 930, 18, doi: [10.3847/1538-4357/ac6262](https://doi.org/10.3847/1538-4357/ac6262)
- Wang, Y., Ji, L., García, J. A., et al. 2021b, *ApJ*, 906, 11, doi: [10.3847/1538-4357/abc55e](https://doi.org/10.3847/1538-4357/abc55e)
- Wijnands, R., Homan, J., & van der Klis, M. 1999, *ApJL*, 526, L33, doi: [10.1086/312365](https://doi.org/10.1086/312365)
- Wilms, J., Allen, A., & McCray, R. 2000, *ApJ*, 542, 914, doi: [10.1086/317016](https://doi.org/10.1086/317016)
- Yatabe, F., Negoro, H., Nakajima, M., et al. 2019, *The Astronomer's Telegram*, 12425, 1
- Zdziarski, A. A., Dziełak, M. A., De Marco, B., Szanecki, M., & Niedźwiecki, A. 2021, *ApJL*, 909, L9, doi: [10.3847/2041-8213/abe7ef](https://doi.org/10.3847/2041-8213/abe7ef)
- Zdziarski, A. A., Johnson, W. N., & Magdziarz, P. 1996, *MNRAS*, 283, 193, doi: [10.1093/mnras/283.1.193](https://doi.org/10.1093/mnras/283.1.193)
- Zhang, G. B., Bernardini, F., Russell, D. M., et al. 2019, *ApJ*, 876, 5, doi: [10.3847/1538-4357/ab12dd](https://doi.org/10.3847/1538-4357/ab12dd)
- Zhang, L., Wang, Y., Méndez, M., et al. 2017, *ApJ*, 845, 143, doi: [10.3847/1538-4357/aa8138](https://doi.org/10.3847/1538-4357/aa8138)
- Zhang, L., Altamirano, D., Cúneo, V. A., et al. 2020a, *MNRAS*, doi: [10.1093/mnras/staa2842](https://doi.org/10.1093/mnras/staa2842)
- Zhang, L., Altamirano, D., Remillard, R., et al. 2020b, *The Astronomer's Telegram*, 13465, 1
- Zhang, L., Méndez, M., Altamirano, D., et al. 2020c, *MNRAS*, 494, 1375, doi: [10.1093/mnras/staa797](https://doi.org/10.1093/mnras/staa797)
- Zhang, L., Altamirano, D., Uttley, P., et al. 2021, *MNRAS*, 505, 3823, doi: [10.1093/mnras/stab1553](https://doi.org/10.1093/mnras/stab1553)
- Zhang, L., Méndez, M., García, F., et al. 2023a, *MNRAS*, 526, 3944, doi: [10.1093/mnras/stad3062](https://doi.org/10.1093/mnras/stad3062)
- Zhang, Y., Méndez, M., García, F., et al. 2022, *MNRAS*, doi: [10.1093/mnras/stac690](https://doi.org/10.1093/mnras/stac690)
- . 2023b, *MNRAS*, 520, 5144, doi: [10.1093/mnras/stad460](https://doi.org/10.1093/mnras/stad460)
- Życki, P. T., Done, C., & Smith, D. A. 1999, *MNRAS*, 309, 561, doi: [10.1046/j.1365-8711.1999.02885.x](https://doi.org/10.1046/j.1365-8711.1999.02885.x)